Fabrication and Analysis of Mixed Matrix Membrane utilizing Metal Organic Framework (MOF-74) in PDMS for CO_2 Gas Separation

By

Subhan Ali

School of Chemical and Materials Engineering

National University of Sciences and Technology

2023

Fabrication and Analysis of Mixed Matrix Membrane utilizing Metal Organic Framework (MOF-74) in PDMS for CO_2 Gas Separation

Name: Subhan Ali

Registration No: 00000328888

This thesis is submitted as a partial fulfillment of the requirements for the degree of

MS in Chemical Engineering

Supervisor Name: Dr. Sarah Farrukh

School of Chemical and Materials Engineering (SCME)

National University of Science and Technology (NUST)

H-12, Islamabad, Pakistan.

March, 2023

Dedication

My unfailing sources of support and direction are honored in this study. My parents, whose direction and encouragement have been crucial, my supervisor, who has offered expertise, counsel, and encouragement, and my lab colleagues, with whom I have shared fantastic experiences while working together.

Acknowledgements

With deep gratitude to Almighty Allah, who bestowed upon us the ability to think and explore the vast universe, this research work is dedicated to Him. Countless praises and blessings are upon the Holy Prophet Hazrat Muhammad (PBUH), who is the reason for the creation of the universe and the source of knowledge and blessings for all humankind.

I would like to express my heartfelt appreciation to my research supervisor, **Dr. Sarah Farrukh**, for her unwavering technical and moral support throughout my research journey. She has been a guiding light, inspiring me to strive for excellence and pushing me to pursue a research vision. Her pursuit of perfection and commitment to excellence has been a constant source of motivation for me.

I am deeply grateful to my Guidance Examination Committee (GEC) members, **Dr. Tayyaba Noor** and **Dr. Erum Pervaiz**, for their invaluable guidance and support throughout my research work. Without their help, this research would not have been possible.

My seniors also deserve a special mention, for their knowledge sharing and motivation throughout the research process. The supportive staff of SCME also coordinated with me seamlessly, enabling me to work with different equipment with ease.

Last but not least, my heartfelt gratitude goes to my parents, whose love, support, and encouragement have been my driving force in pursuing my goals. Words cannot express the depth of their sacrifice and effort towards shaping my life.

Subhan Ali

Abstract

The fabrication of mixed matrix membranes (MMMs), which contain metal-organic frameworks (MOFs) of Ni and Cu-MOF-74 with rubbery polydimethylsiloxane (PDMS) polymer matrix, is a response to the growing concern about carbon dioxide (CO_2) emissions. These membranes have a lot of potential to separate gases because of the hydrophobicity, high gas permeability, and flexibility of PDMS, as well as the substantial effective areas and distinctive characteristics to adsorb gas by MOFs. In order to maximize CO_2 separation and CO_2/N_2 and O_2/N_2 selectivities, this work describes the manufacturing procedure of MMMs with different concentrations of Ni and Cu-MOF-74 (0.5%, 1%, 1.5%, and 2%). To get understanding of the behavior of the MOFs and MMMs, the characterization using XRD, SEM, FTIR, and mechanical strength testing was conducted. Following analysis, it was determined that 1wt%Ni-MOF-74@PDMS and 1wt%Cu-MOF-74@PDMS were the best MMMs because of their uniform MOF dispersion into the polymer matrix, which was determined by SEM-EDX mapping, high tensile strength, and increased CO_2 permeation to 4288 Barrer (34% increase) and 4432 Barrer (40% increase), respectively. Moreover, 1wt%Cu-MOF@PDMS demonstrated an increase in CO_2/N_2 and O_2/N_2 selectivity to 94.7 (428% increase) and 6.47 (150% increase), respectively, whereas 1wt%Ni-MOF@PDMS showed an increase in CO_2/N_2 and O_2/N_2 selectivity to 36.2 (125% increase) and 3.2 (25% increase). The Lewis acidic sites of MOF-74-NCs for CO_2 and O_2 as well as the presence of porous fillers are both credited with this increase in selectivity. In conclusion, this work offers insightful information on how MOF chemistry affects membrane permeability and selectivity, which may have important ramifications for the advancement of gas separation technologies.

Table of Contents

List of Figures

List of Tables

List of Acronyms

MMM	Mixed Matrix Membrane	%	Percentage
MOF	Metal Organic Framework	PU	Polyurethane
PDMS	Polydimethylsiloxane	NCs	Nano Crystals
Ni	Nickle	vol.	Volume
Cu	Copper	Fig.	Figure
CO2	Carbon Dioxide	µm	Micrometer
O2	Oxygen	cm	Centimeter
N2	Nitrogen	kV	Kilo Volt
SEM	Scanning Electron Microscopy	º	Degree
XRD	X-ray Diffraction	kW	Kilo Watt
EDX	Energy Dispersive X-Ray	mA	Mili Ampere
UTS	Ultimate Tensile Strength	mm	Mili Meter
FT-IR	Fourier-transform infrared spectroscopy	min	Minute
MWCNT	Multi Walled Carbon Nanotubes	kN	Kilo Newton
ASTM	American Society for Testing and Materials	Wt.	Weight
P	Permeability	℃	Degree Celsius
IPCC	Intergovernmental Panel on Climate Change	H	Hydrogen
Si	Silicon	Δ	Differential
CH3	Methane	L	Thickness
$Si(CH_3)_2O$	Polydimethylsiloxane	A	Area
FFV	Fractional Free Volume	p	Pressure
ZIF	Zeolitic imidazolate frameworks	α	Ideal Selectivity
Mg	Magnesium	nm	Nano Meter
Co	Cobalt	C	Carbon
Mn	Manganese	-O	Oxygen Bond
OH	Hydroxyl	>	Greater Than
Q	Volumetric Gas Flow Rate	MPa	Mega Pascal

Chapter 1

Introduction

1.1 Background

Due to industrial manufacturing of commodities to suit the demands of the global community, energy consumption is quickly rising as the world's population continues to expand. Energy is needed for the increased industrial production. Petroleum derivatives including combustible gas, coal, and lubricants account for around 64% of the world's power energy needs. Due to their finite reserves and rapid depletion, fossil fuels cause problems for the economy and ecology. Resource depletion and climate change brought on by the use of fossil fuels have made it clear that switching to another energy system is required [1].

During the industrial revolution, the amount of CO_2 in the atmosphere has increased significantly over the last 200 years. The worldwide carbon-based project's estimated CO_2 concentration increased by 2.7 percent in 2018. In 2018, CO_2 emissions from fossil fuels totaled 37.1 billion metric tons. The earth gets 1.50C hotter as a result of this increase in CO_2 emissions. The consequences for our planet might be hazardous if CO_2 emissions continue at this rate [2]. However, the outlook for the fossil fuel energy system is not encouraging. Their reserves have already reached their maximum levels. The US Department of Energy has anticipated that coal, natural gas, and oil will last 100, 150, and 50 years, respectively. There are no fresh reserves being found. The prediction for the global energy usage rate, however, is not a positive one because it assumes that by the end of 2050, demand would have practically doubled [3, 4].

The global energy consumption of individuals is about 13 TW. To meet this enhancing demand for energy globally and maintain a low level of atmospheric CO_2 concentration. According to Hoffert et al., it will need the production of 15, 25, and 30 TW of carbon-free energy to keep the atmospheric CO_2 concentration at 550, 450 and 350 ppm, respectively, by 2050 [5].

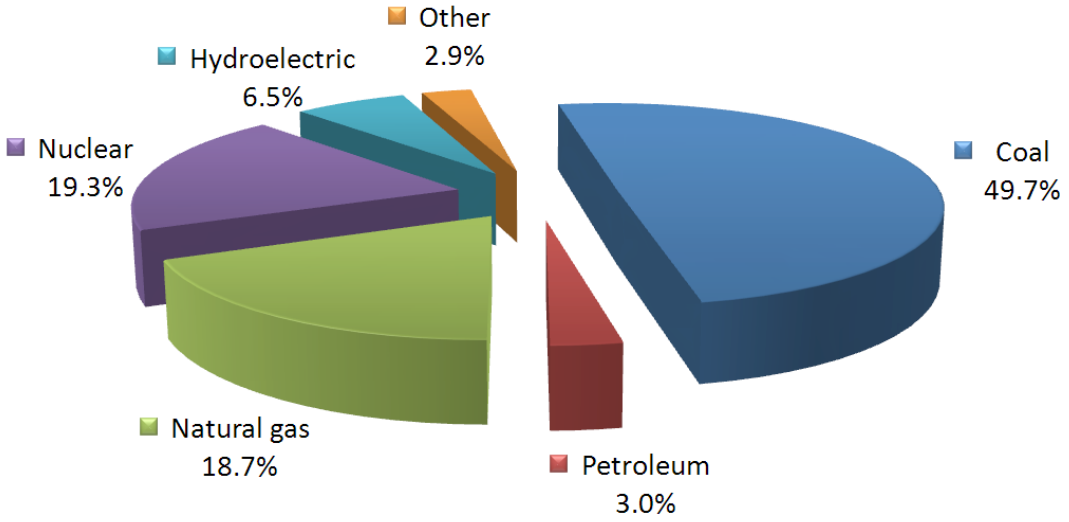

Figure 1: Percentage contribution of different sources used for power generation [2]

A significant energy source for both businesses and homes is natural gas. Methane makes up the majority of natural gas's combustible components, with modest amounts of ethane and propane. Together with the principal constituents, natural gas also contains a sizable number of impurities, including CO, H_2S, SO_2, and CO_2 [6]. As an illustration, the following is a summary of the natural gas composition found in Malaysia (Table 1). Wasiu et al. claim that when compared to pure natural gas, increasing carbon dioxide levels are observed to lower the natural gas heating value. This has been demonstrated in many tests using a variety of natural gas mixes that contained various concentrations of CO_2. It was observed that the heat produced by the reaction and the speed of combustion reduced as the amount of CO_2 rose [7]. Also, as the world population grows, so does the need for energy. Between 1990 and 2020, it is predicted that the world population would rise by a factor of 1.1%, whilst the energy consumption will rise by 2.2% [8]. In a different estimate conducted in 2000 for 14 EU countries, the relationship between energy consumption and population was examined, and Table 2 illustrates the pattern that showed population growth and energy consumption rose concurrently [9].

Table 1: Composition of compressed natural gas (CNG) used in Malaysia [7]

Component	Volume percentage (vol%)
Methane	94.42
Ethane	2.29
Butane	0.25
Nitrogen	0.44
Carbon dioxide	0.57
Others	2.00
Propane	0.03

Table 2: Correlation between population (in thousands) and energy consumption (in thousands of metric tons of oil equivalent) [9]

Year	Population	Energy consumption
2000	376,037	1,460,284
2025 – Lower	374,902	1,805,297
2025 – Medium	393,659	1,953,477
2025 – Higher	412,144	2,101,007

Thus, a growth in population necessitates an increase in energy production, which calls for an increase in fuel supplies. Because the gasoline we now have is already running out very quickly. According to studies done by N.A. Owen et al., oil reserves increased in the early 1900s, particularly from 1930 onwards. But, after 1972, the oil supplies began to run out. This indicates that more oil was extracted from the reservoirs than was discovered there. Around 1980, the reserves were steadily running out, which showed that there were less conventional energy supplies available [10]. As we've already shown, adding CO_2 lowers the energy output of fuel gases. So, if we want to enhance the output from traditional energy sources, we must lower the CO_2 content of the natural gas being utilized.

1.2 Requirements of CO_2 Separation

We have several ways, such as gas absorption through liquids and gas adsorption on solid surfaces, to separate CO_2 from other gases, including natural gas [11], and membrane gas separation [12]. The most advanced and deemed most acceptable approaches for CO_2 separation are liquid gas absorption and adsorption on solid surfaces. These two techniques for petrol separation are widely employed in the business. The biggest disadvantage of these two procedures is that they both need a lot of energy, but there are other disadvantages as well. This indicates that the additional energy required to remove or capture the carbon dioxide gas balances out the energy gained from natural gas by lowering its carbon dioxide level [13].

1.2.1 Pressure swing Adsorption (PSA)

PSA is based on the structural and functional characteristics of adsorbent materials, which under high pressure generated a stronger physical connection with the adsorbate impurities. The removal of contaminants from input streams involves the use of a variety of materials. Table 03 lists several adsorbents and their corresponding adsorbing impurities. Large fixed beds in the shape of cylinders make up the PS unit. Under high partial pressure, the contaminants from reactors are adsorbed inside these beds. While adsorbents are being renewed, these pollutants are then discharged from the beds at low pressure. The PSA process consists of five basic phases in general.

1. Adsorption
2. Concurrent depressurization
3. Countercurrent depressurization
4. Purge
5. Repressurization

In the PSA process, high pressure feed gas containing impurities is introduced, and these impurities are subsequently confined inside the beds, resulting in high purity hydrogen at the product sides. To provide a continuous flow of feed and product, several adsorber are employed in parallel and series. Fresh adsorbers are provided with feed gas each time. These contaminants begin to saturate the adsorber. The adsorber is simultaneously

depressurized during the next stage to remove the last hydrogen that was trapped inside the adsorber beds during the first step. During the countercurrent depressurization process, the adsorber underwent partial regeneration to remove the contaminants. The beds are fully restored in the fourth phase by removing the hydrogen that was purged in the second step. The feed stream repressurized the adsorber together with some of the product and hydrogen taken from the next stage to keep the adsorber at the proper pressure. The cycle is then repeated by starting a process. the 200kPa-or-less hydrogen collected from the product side. Recompression after transit and transportations need additional energy. Hence, this approach is not appealing for the filtration of gases [14-16].

Table 3: Materials used for pressure swing adsorption [14]

Adsorbent materials	**Adsorbates**
Silica gel	Water, CO_2, hydrocarbons
Activated carbon	CO_2, CH_4, N_2,
Molecular Sieve (Zeolites)	CH_4, CO_2, N_2
Alumina oxides	water
Carbon molecular sieve	O_2

1.2.2 Cryogenic Distillation

The boiling point of the input gases was used as driving force in cryogenic distillation. It is a commercially accessible low temperature process. The ability of the procedure to create liquid hydrogen that is ready for shipment is its main benefit. Moreover, no chemical reagents are employed in this procedure. Compared to other acidic gases, hydrogen has a substantially lower boiling point. Hydrogen must be liquefied using a high-energy refrigeration system since its boiling point is substantially lower. The main

limitations of the cryogenic process are the high capital and operating costs and process pore blockage. Cryogenic distillation is also not practical on a small scale [17, 18].

1.2.3 Membrane Technology

Membranes are basically known as semi-permeable barriers that permit one of the elements from a gaseous mixture to pass through while keeping others. The petrol separation mechanism is driven by pressure gradient and chemical potential. Membrane has attracted a lot of attention from researchers because of its affordability, environmental friendliness, and ability to be used in both small- and large-scale applications. The membranes are divided into two categories, inorganic and organic, depending on the materials they are made of. Whereas organic membranes are formed of polymers, inorganic membranes are further divided into ceramic and metallic membranes. There are three mechanisms that allow gases to move across membranes: solution diffusion, molecular sieving, and Knudsen diffusion. Gas will convectively flow through a membrane if molecules have a considerably smaller kinetic diameter than the holes, which will reduce selectivity. Via a molecular sieving process, the large-diameter molecules are filtered out to separate the gases. Most often, this kind of technique is used to separate specific gas using microporous membranes. On the other side, the dense membranes are used in the solution diffusion mechanism to controls the separation of gases. The solution diffusion model consists of three steps. (1) Gas molecule absorption on membrane surface on the high-pressure side, (2) Gas diffusion across membrane, and (3) Gas molecule desorption on low pressure side. On the other hand, gas molecules binds to the surface of metallic membranes and separates into atoms. Next, at the product side, these atoms cross a membrane and rejoin to create complete gas molecules. Dense ceramic membranes allow gas ions and electrons to pass through them. In comparison to other membranes, high temperature is necessary to achieve high penetration flux through ceramic, metallic, and composite ceramic-metallic membranes. It will take a lot of energy to do this. Based on the two variables of ideal selectivity and permeability, the separation produced from various sources is assessed. Membrane having higher selectivity will separate more efficiently with a higher degree of purity. Conversely, a membrane with high permeability produces well. The two parameters diffusivity and solubility combines the effect of the

parameter of membrane. Due to its non-polarity and lowest kinetic size among other gas molecules, hydrogen has a lower solubility coefficient and a higher diffusion coefficient than other gas molecules [19, 20].

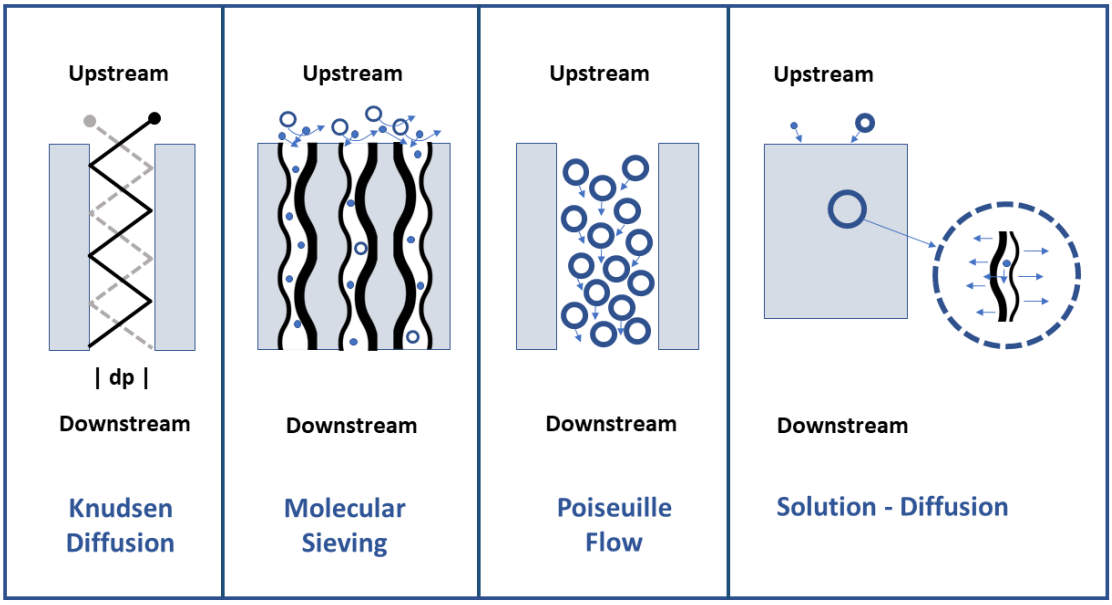

Figure 2: Gas transport mechanism through membrane a) Knudson diffusion b) Molecular sieving c) Poiseuille Flow d) Solution diffusion [19]

1.3 Introduction to Mixed Matrix Membranes

Polymeric materials and inorganic filler particles combine to produce a single continuous matrix, which is what MMMs are made of [21]. The inorganic filler particles may include zeolites [22], metal-organic frameworks [23] and carbon molecular sieves [24] among others. As will be discussed in following chapters with proper citations to published material, these particles when introduced into the structure of membranes are known to increase the ideal separation behavior and the overall performance of original membranes

1.4 Introduction to Metal-Organic Frameworks (MOFs)

MOFs are a group of porous, polymeric solids that are held together by organic ligands that connect metal ions. The majority of MOFs are crystalline solids, however depending on how connections are created, they can also have one-, two-, or three-dimensional

structures. Because of the repeating pattern of metal ions and organic ligands kept in place by coordinated covalent bonds, they can also be referred to as co-ordination polymers. Depending on the differences in the size of effective pores and the kinetic diameter of the different gas molecules, these links between metal ions and organic linkers give birth to distinct pores that can trap some gases while allowing other gases to flow through. There are many applications for MOFs. Some of these applications can be summarized as follows:

- Gas separation, storage and capture [25]
- Gas sensing and detection, and advanced catalysis [26]
- Biotechnology and microelectronics [27]

We are mainly interested in the usage of MOFs for the separation of gases among these applications. As was previously mentioned, metal organic frameworks include MOF-74 as a subcategory (MOFs). They get their moniker because to the way they are built. MOFs are created by joining imidazole linking groups with transition metal ions (Cu, Ni).

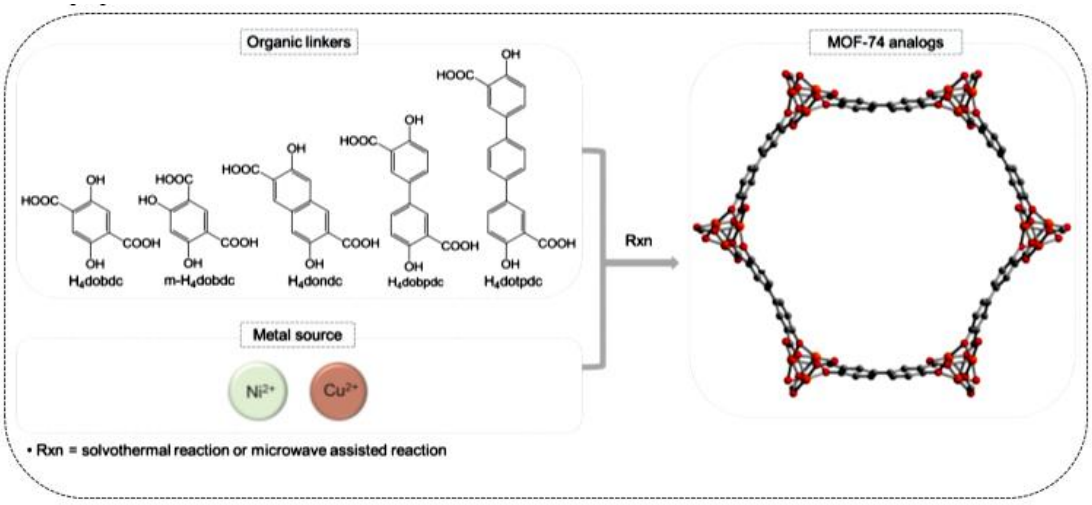

Figure 3: Chemical Structure of Cu-MOF-74 & Ni-MOF-74 [28]

1.5 Introduction to polydimethylsiloxane (PDMS)

The membrane material is the key factor in efficient gas separation [29]. Polymeric membranes for gas separation have grown in popularity because of their improved processability, financial potential, and mechanism of operation [30]. Many different polymers (glassy and rubbery) have been investigated as the primary material for membrane separation techniques [31]. A potential polymeric membrane to be used for gas separation is the (polydimethylsiloxane) $-Si(CH_3)_2O-$ (PDMS) membrane because of its hydrophobicity, high gas permeability, sizable free volume, high mechanical strength and flexibility, comparative affordability, and excellent chemical and thermal stability [32, 33].

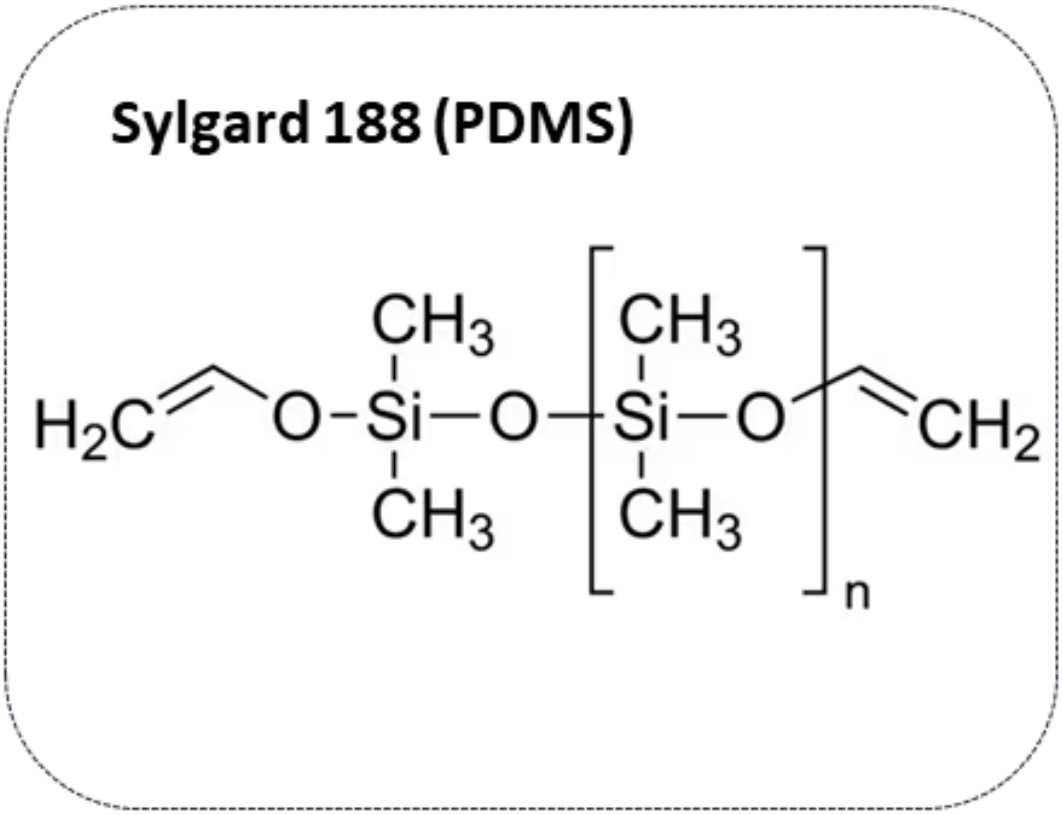

Figure 4: Chemical Structure of Polydimethylsiloxane (PDMS) (Sylgard® 184 Silicone Elastomer) [33]

1.6 Use of MOFs in Mixed Matrix Membranes

As previously mentioned, MOFs have remarkable porosity and tunable pores, making them suitable for usage as filler particles distributed in the bulk phase, or main matrix, of a membrane. Depending on our use and the operating circumstances the membrane is to be subjected to, the major matrix or bulk phase may be polymeric, ceramic, or glass. Even at such low concentrations, MOFs have proved to have outstanding separation qualities when utilized in the bulk membrane phase [34].

1.7 Motivation

We are interested in learning more about MOF-74's impact on the passage of CO_2 via a membrane. Moreover, we are interested in the impact of altering the filler particles into polymer matrix of membranes on the penetration selectivity of CO_2 relative to O_2 and N_2. In order to increase the selectivity for CO_2/O_2, CO_2/N_2, and O_2/N_2 in a PDMS mixed matrix membrane, this effort will utilize (Cu and Ni) MOF-74. This is done to make better use of the already available resources in order to tackle the ongoing energy crisis. Also, it lessens the strain on resources and restricts the negative human activity effects on our environment.

1.8 Objective

My research objectives are:

- Fabrications and Optimization of MOF-74/PDMS MMM.
- To fabricate (Cu, Ni) MOF-74 based mixed matrix membranes.
- Investigate the advantages fabricated MMM over pure PDMS membranes, as well as the impact of MMMs on the membrane's ideal selectivity and optimum permeability.
- Characterization of the resulting membranes using the following methods
    1. Scanning Electron Microscopy (SEM)
    2. Fourier Transform Infra-red (FT-IR) Spectroscopy
    3. Energy-dispersive X-ray spectroscopy (EDX)
    4. X-Ray Diffraction (XRD)

5. Ultimate Tensile Strength (UTS)

- As a last step, we compare the performance of all fabricated MMMs and pristine PDMS membranes to get the optimum separation, and we make recommendations for future developments based on the comparison's findings.

Chapter 2

Literature Review

As carbon dioxide is a non-combustible gas, it must be removed from the natural gas extracted from the reservoirs since it lowers the overall gas reserves' energy content. There are several types of membranes that may be utilized for this, however mixed matrix membranes are the most often studied ones by researchers [35].

2.1 Applications of MMMs

There are numbers of applications regarding Mixed Matrixes like wire and cable insulation, automobile interiors, and appliance housings for a long time [36]. MMM have, however, recently discovered uses in the creation of gas separation membranes [37]. They comprise both the solid filler and polymer base membranes that are created when such membranes are created. The goal of MMMs is to provide the membranes certain characteristics that would improve their ability to isolate a specific component of a mixture while yet being selective. Because some group like -NH_2 and -OH are known to favorably adsorb carbon dioxide in any material, adding basic groups to the membrane in our case is necessary. Ths removal is made possible because to this technique [38].

2.2 Use of MMM for gas separation

Mixed matrix membranes are the membranes created by this modification approach (MMMs). MMMs provided features that combined filler and polymer characteristics. Because of their customizable pore shape, which offers outstanding separation performance, MOFs and ZIFs have emerged as an appealing inorganic filer. The thermal and mechanical stability of mixed matrix membrane was improved by both of these factors and their interaction with the polymer interface.

2.3 Use of MOFs for gas adsorption and separation

Metal organic frameworks have been employed in the field of petrol separation for many years, as was previously mentioned. This use of MOFs is made possible by various advantageous MOF characteristics, which will be discussed in this article. Selective adsorption of one gas relative to another is the method used for gas separation when utilizing MOFs alone [39]. In this regard, Chen et al. created the Bio-MOF-11 biological MOF and evaluated its ability to adsorb CO_2, O_2, and N_2. The gas mixture's CO_2/H_2 adsorption selectivity is found to be between 230 and 375, whereas the gas mixture's CO_2/N_2 adsorption selectivity is found to be between 30 and 77 [40]. Other study by Li et al. evaluated the selective gas adsorption of MOF-177, a metal organic framework (MOF) made of zinc benzene-tri-benzoate. With a selectivity of 1.8 vs 1.5 wt%, this demonstrated that O_2 have been adsorbed more selectively to N_2 [41].

Because of the favorable affinity between basic amine groups and acidic carbon dioxide gas, as was previously mentioned, functionalized MOFs specially with amine are particularly well suited for adsorption of CO_2 gas .McDonald et al. conducted a specific study in this area. In this study, a unique MOF with the general formula m^2(dobpdc) was created and modified to create the amine functionalized MOF (dobpdc). The resultant MOF exhibits CO_2/N_2 adsorption selectivity values for flue gases is 200 and 49000 from air. [42]. Once it was discovered that MOFs with amine-functionalization had a greater capacity for carbon capture. Tetra-ethylene-pentamine (TEPA) was used to modify a MOF called MIL-101 in one such study by Wang et al., resulting in TEPA-MIL-101. For CO_2/CO separation, both unmodified and modified MOFs were employed. The resultant product had a higher CO_2 adsorption capacity while having a much lower CO adsorption capacity. The amine functionalization also increased the CO_2/CO adsorption selectivity from 1.77 to 70.2 [43].

2.4 Incorporation of MOFs in membranes

Over a long period of time these polymer membranes have been employed to separate number of gases, but their usefulness has always been constrained. Yet when MMMs are created, they would have combine benifits of organic polymeric chains with inorganic fillers [44]. Similar research is being conducted using MOFs that have been introduced into polymer chain matrix. In a study, Basu et al. created a mixed matrix membrane with a Matrimid and by varying MOF concentrations known as MIL-53(Al), varies from 0 to 30%. Findings revealed that increasing filler loading increases CO_2 permeance by up to 218%, while also increasing CO_2/CH_4 selectivity, which rose and was in the 28–35 range [45]. In a different research project, Perez et al. created a Matrimid-based MMM using MOF-5 as nanofiller. Which raised permeabilities of the gases by 120% by the addition of MOF-5 to the membrane. The range of the CO_2/N_2 ideal selectivity was demonstrated of 36 to 44 [46].

Similar to how earlier said, MOFs can more easily absorb carbon dioxide when modified with amine groups. These amine-modified MOFs would by their very nature increase the separation efficiency of CO_2 over other various gases when utilized in polymer matrix. In a variety of research efforts, this characteristic of (MMMs) were used to separate CO_2 from air and flue gases. Zornoza et al. examined that the amine functionalized MIL-53 (Al) incorporated into a poly-sulfone membrane to create the final MMM. It has been showing an optimum CO_2/CH_4 selectivity of 45 and significantly improves the separation behavior of CO_2 over other gases [47]. In a related study, M.W. Anjum et al. created MMMs using UiO-66@Matrimid (Filler/polymer matrix). The MOF was functionalized by including amine groups. The resultant MMM showed an optimum values for CO_2/CH_4 selectivity of 47.7, has greater CO_2 separation than an empty (without MOF) Matrimid membrane [48].

2.5 Incorporation of ZIFs in membranes

ZIFs have also been utilised as membranes to facilitate gas separation, much like regular MOFs. In order to create a mix that is ideal for the most efficient gas separation, an emerging area to deal with these researches. In one study by Li et al., ZIF-7@poly (amide-b-ethylene oxide) were coupled to create a MMMs. The resulting MMMs have an optimum CO_2 permeability (PCO_2) of 145 bars, a CO_2/N_2 ideal selectivity of 97, and a CO_2/CH_4 ideal selectivity of 30 [49]. In one experiment, ZIF-8 filler was added above the support layer, and then served as the primary phase, to separate an ethane/ethane combination. At pressures of 1 bar and 6 bar, these MMM showed an ideal selectivities for an ethene/ethane of 2.8 and 2.4, respectively. Two conflicting selectivities are the main causes of the relatively poor selectivity of ethene over ethane [50].

The addition of amine groups to the ZIFs' structures, followed by their incorporation into the membrane structure, can result in various additional advantageous CO_2 separation features. One such study was conducted by Nordin et al., who created the ZIF-8 and used ammonium hydroxide to modify it. Then, the resultant modified ZIF-8 utilized with the poly-sulfone base polymer. The final membrane's permeability and selectivity were evaluated using a CO_2/CH_4 combination, and it was discovered that the CO_2/CH_4 selectivity ranged from 25 to 43 [51]. Huang et al. conducted yet another study on the CO_2 extraction from gas mixtures utilizing amino-modified ZIF MMMs. They created ZIF-90 and used 3-aminopropyltriethoxysilane (APTES) to modify it. The -alumina support was coated with APTES before being submerged in the prepared ZIF-90 solution to create this modified ZIF-90 filler. As a result, ZIF-90 membranes are amino-modified. The next step is to test the membrane for gas transport and separation, for which, a 50:50 CO_2/CH_4 combination is employed. In the study, the CO_2/CH_4 selectivity reached 4.7 [52].

2.6 Incorporation of different fillers into PDMS polymer matrix

Comparing this research's CO_2/O_2 selectivity, CO_2/N_2, and CO_2/O_2 separation efficiency to that of other studies that employed polymers with identical structures but different fillers. High performance was reportedly attained in the CO_2 and O_2 separation procedures, according to recent experiments utilizing ZIF-8 nanofillers [53, 54]. For instance, high CO_2 permeability (Barrer) 53.69 and O_2 permeability (Barrer) of 13.42 with increased CO_2/N_2, O_2/N_2, and CO_2/O_2 separation selectivity of 22.37, 5.5, and 4, respectively, were achieved employing 2 wt.% thermally annealed ZIF-8 nanofiller in a PDMS polymer matrix [55]. Another study by E. Roh et al. [56], the best CO_2/N_2 separation characteristics were found to be 17.60, 17.90, 14.50, and 18.00, respectively, with a CO_2 permeability of 1608, 1508, and 1468 Barrer, and an O_2 permeability of 268, 336, and 339 Barrer, respectively, when M-MOF-74 (M = Mg, Co, Ni, and Mn) was used in the PDMS polymer matrix. [28]. Similarly, EA Silva et al. [57], utilized 1 wt.% MWCNT in a PDMS polymer matrix to produce an optimum separation selectivity CO_2/N_2 and O_2/N_2 ideal selectivity values of 11.83 and 2.81, respectively, having a maximum CO_2 permeability (Barrer) of 1500 and O_2 permeability (Barrer) of 540. Moreover, M. A. Semsarzadeh et al. [58], recently reported using 1 weight percent silica in the PU-PDMS blended polymer matrix to get an optimum CO_2/N_2, O_2/N_2, and CO_2/O_2 ideal selectivity values of 64.4, 4.7, and 13.8 respectively, with a maximum CO_2 permeability (Barrer) of 96 O_2 permeability (Barrer) of 7. In a certain Table (9) at particular pressures, these literature data are contrasted with the results of our study.

Table 4: Literature review relating to MOFs and amino-modified MOFs

Metal organic Frameworks (MOFs)	**Selectivity**	**References**
Bio-MOF-11	CO_2/N_2 = 30-77	[40]
MOF-177	O_2/N_2 = 1.8	[41]
Mmen-Mg_2(dobpdc	CO_2/N_2 =49000 (from air) CO_2/N_2 = 200 (from flue gases)	[42]
TEPA-MIL-101	CO_2/CO = 70.2	[59]

Table 5: MOF and amino-modified MOF based mixed matrix membranes

Polymer	**Filler**	**Selectivity**	**References**
Matrimid	MIL-53 (Al)	CO_2/N_2 = 36-44	[45]
Matrimid	MOF-5	CO_2/CH_4 = 40-51	[46]
Polysulfone	NH_2-MIL-53	CO_2/CH_4 = 45	[47]
Matrimid	Zirconium terephthalate UiO-66 modified by 2-aminoterephthalic acid and 4-aminobenzoic acid	CO_2/CH_4 = 47.7	[48]

Table 6: Literature review of ZIFs and amino modified ZIFs

Zeolitic Imidazolate Frameworks (ZIFs)	**Selectivity**	**Reference**
ZIF-95 ZIF-100	H_2 uptake capacity = 3.5 wt% H_2 uptake capacity = 10.5 wt%	[60]
Amine-modified ZIF	Increased in O_2capacity by 199.6%	[61]
ED-ZIF-8	CO_2/N_2 = 23	[62]

Table 7: Literature review of ZIF and amino-modified ZIF based mixed-matrix membrane

Matrix material	**Filler**	**Selectivity**	**Reference**
Pebax 1657 Arkema	ZIF-7	CO_2/N_2 = 97	[49]
Titania-alumina support	ZIF-8	Ethene/ethane = 2.8	[50]
Polysulfone	ZIF-8 modified using ammonium	CO_2/CH_4 = 25-43	[51]

Table 8: Literature review of polymer blend membranes

Continuous phase	Dispersed phase	Selectivity	Reference
Polysulfone	Polyimide	O_2/N_2 = 6-7, CO_2/N_2 = 25-30	[63]
Polyvinyl alcohol	Polyallyl amine	CO_2/N_2 = 80 CO_2/CH_4 = 58	[64]
Victrex 4800P	Radel A-300	He/N_2 = 4.58	[65]
Cellulose acetate	Polyethylene glycol	CO_2/N_2 = 36.2	[66]

Table 9: Comparison analysis data of the gas (CO_2 and O_2) separation efficiency of different recently reported membranes in the literature with this present research work [58]

Membrane	**Filler**	**Pressure (Bar)**	**PCO_2 (Barrer)**	**PO_2 (Barrer)**	**Selectivity (CO_2/N_2)**	**Selectivity (O_2/N_2)**
PDMS	N/A	1.1	3180	N/A	8.8	N/A
PDMS	ZIF-8-CNT	1	8705	N/A	45.6	N/A
PDMS	1 wt.% MWCNT	0.96	1500	540	11.83	2.81
PDMS	40 wt.% UiO-66-NH_2	2	2500	N/A	18	N/A
PIM-1	PDMS@MOF-74-Ni Gutter layer	1	5015 GPU	N/A	31	N/A
PDMS	N/A	4	2281	571	8.5	2.1
PDMS	Mg-MOF-74-NC	4	1608	268	17.6	2.9
PDMS	Mn-MOF-74-NC	4	1468	339	18	4.2
PDMS	Co-MOF-74-NC	4	1508	336	17.9	4.0
PDMS	Ni-MOF-74-NC	4	1502	278	14.5	2.7
PDMS	N/A	-	3395	N/A	11	N/A
PDMS	KIT-6 silica	0.5	12	N/A	1.9	N/A
PDMS	2% Thermal annealed ZIF-8	3	53.69	13.42	22.37	5.5
PU-PDMS	10 wt.% Silica	10	96	7	64.4	4.7

Chapter 3

Material and Method

3.1 Materials

The Dow Chemical Company created polydimethylsiloxane (PDMS) (Sylgard® 184 Silicone Elastomer). We bought the polymer (PDMS) and the toluene solvent from Sigma Aldrich. Paradise Corporation, Pakistan, provided lab scale high purity CO_2 (>99.999 vol%), N_2 (>99.995 vol%), and O_2 (>99.999 vol%) gases. All of the chemicals and solvents utilized in this investigation were of the analytical kind and were not previously purified [34].

3.2 Preparation of Pristine Membrane

The solution casting process was used to create pristine membrane. Toluene is employed as a solvent and PDMS is used as a polymer. Kept the optimum ratio of 10:1 of base elastomer and curing agent to make the rubbery PDMS polymer matrix. A certain amount of toluene solvent was mixed continuously at 300 rpm for two hours at room temperature before PDMS 40 weight percent was added. All the possible air bubbles were removed by the proper degassing of solution in bath sonicator for 30 minutes. The created homogeneous solution mixture is then cast in a petri dish and heated to 80°C for 2 or 3 hours in a hoover drying oven. This membrane was extracted from a petri dish using a surgical blade after it had fully dried. To fit the synthesized membrane in the gas permeation testing apparatus, it was cut in given dimensions according to the rig.

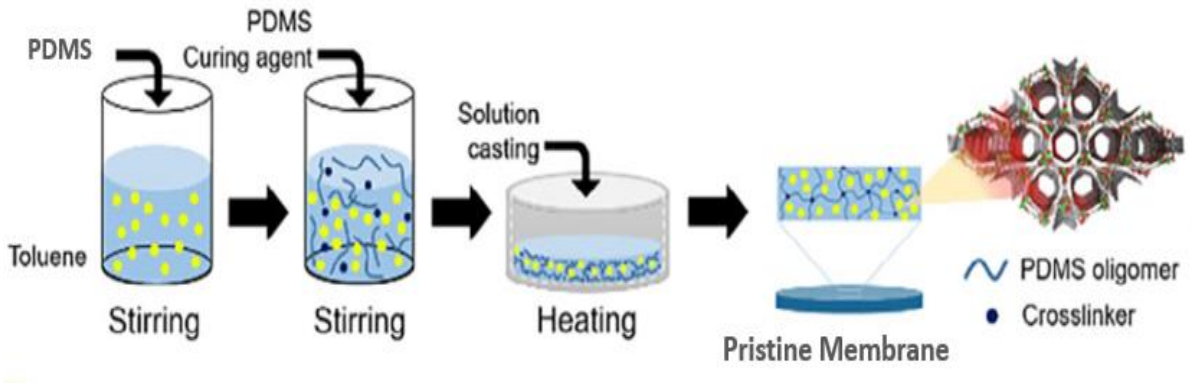

Figure 5: Fabrication of pristine membrane [67]

3.3 Fabrication of Mixed Matrix Membranes (MMMs)

The MOF-74/PDMS MMMs were made using the same solution casting method as before, with the addition of changing the concentration of Cu, Ni-MOF-74 nanofiller in the polymer matrix.

During two hours at room temperature, toluene solvent was continuously agitated at 300 rpm while receiving a 40-weight percent addition of PDMS. In PDMS, the proportion of base elastomer to curing agent is 10:1. MOF-74 was dissolved in toluene at various concentrations between 0.5 and 1 weight percent before being subjected to an hour-long sonication bath. The PDMS solution based on toluene was then mixed with this MOF-74 distributed solution. To avoid filler buildup and sedimentation, continue sonicating in the bath for an extra hour. To get rid of any potential air bubbles, the solution was subjected to a degassing procedure.

The final homogeneous solution is then casted on a petri dish or glass plate and then dried for almost two hours at around 80°C in a vacuum drying oven. Before removing the artificial membranes from the petri dishes using a surgical blade, they were thoroughly dried. The manufactured membranes are 170um (+-10) thick. After that, the manufactured membranes underwent characterization and gas permeation testing. The schematic for the synthesis of PDMS MMMs containing MOF-74 is depicted in the figure below. Table 10 details the membrane preparations' composition.

$$Filler\ Loading\ (wt\%) = \frac{\text{Wight of the Filler}}{\text{Weight of the Filler+Weight of the Polymer}} \times 100 \qquad (1)$$

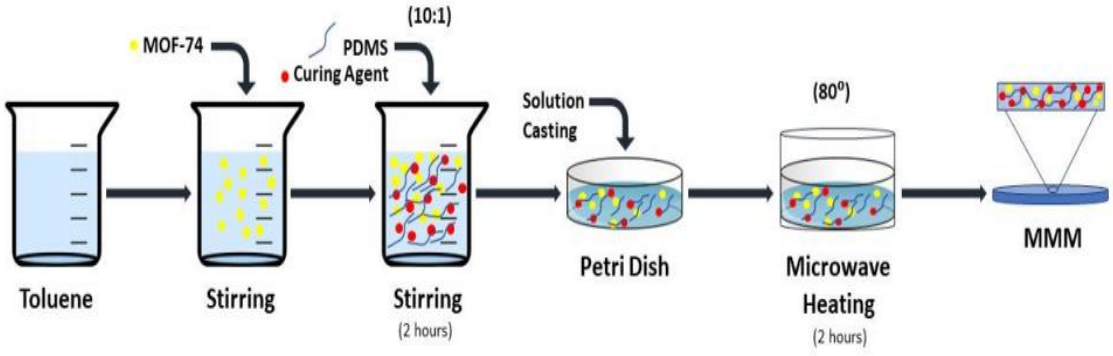

Figure 6: Fabrication of MOF-74/PDMS MMMs [67]

Table 10: Prepared membranes composition (values in wt %).

Names	Polymer PDMS	Solvent Toluene	MOF-74
M_0	10	90	0
$M_{0.5}$	10	89.5	0.5
M_1	10	89	1
$M_{1.5}$	10	88.5	1.5
m^2	10	88	2

3.4 Testing and Characterization

3.4.1 X-ray Diffraction Analysis

XRD, a nondestructive process, may analyze the crystalline or amorphous structure of material and their chemical content along with its physical properties. Its foundation is crystalline samples and monochromatic X-ray interference that is constructive. Shorter wavelength electromagnetic radiation known as X-rays is created when electrically charged particles with sufficient energy are slowed down. A focused and regulated beam

of X-rays is directed at a sample of a nanomaterial during X-ray diffractogram analysis (XRD). A diffraction pattern is produced by the diffracted rays that are produced when these X-rays interact with the material. The structure and characteristics of the material may be investigated by examining the intensity of the diffracted rays at various angles [68]. Here are the three main parts of XRD equipment:

1. X-Ray source
2. Holder
3. X-Ray Detector

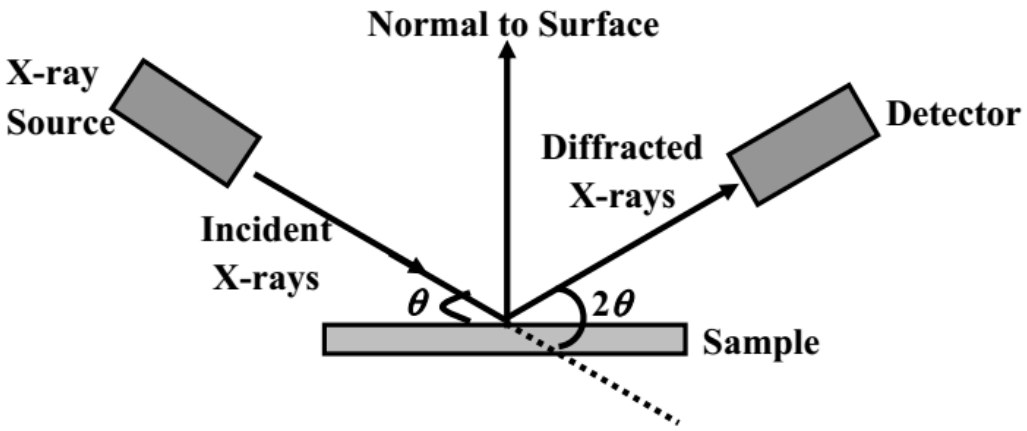

Figure 7: Schematic diagram of XRD [69]

Long-range ordered periodic arrays can scatter light in a way that produces constructive interference at specific angles, leading to diffraction, when they are present in a material. Light can also be diffracted by a crystal depending on the periodic arrangement of its atoms. Due to the fact that, we can compare the wavelength of these X-rays among the spacing of atoms, X-ray Diffraction (XRD) methods make use of this feature to expose the crystalline structure of materials. The arrangement of atoms in crystals may be learned a lot from the X-ray diffraction patterns that are created by atomic scattering of X-rays. Since they don't have a periodic array with long-range order, glass and other amorphous materials don't show any noticeable peaks in the diffraction pattern.

By constructive interference, these interactions produce strong reflected X-rays when Bragg's Law is satisfied. This law explains the connection between the atoms' crystal lattice planes' spacing, incidence angle, and wavelength.

$$n\lambda = 2dsin\theta \tag{2}$$

All phases of the material creates a unique pattern due to its chemistry and atomic structure. The diffraction pattern is created by just adding the diffraction patterns from each phase. A diffraction pattern's peak location depends on the wavelength. The number of X-rays observed at a specific peak or the absolute intensity can both be influenced by experimental and instrument factors. Diffractometers can be employed in transmission or reflection modes [70].

Figure 8: XRD apparatus [70]

Cu K monochromatic radiations were employed in an XRD experiment using a Shimadzu AG-XEUS X-ray diffractometer. An XRD pattern was acquired in the range of 0-80° with increments of 0.04° and 1 sec to observe the structural characteristics of all these fabricated samples. Kept the 20kV voltage, while the tube current was 5mA [70].

3.4.2 Fourier Transform Infrared Spectroscopy

An Infrared light is used in FTIR (Fourier Transform Infrared) examination to scan samples and detect chemical, inorganic, and polymeric materials. When the content of a material varies, the typical pattern of the absorption bands shifts, making it possible to identify unknown substances, contaminants, additions, breakdown rates, and oxidation rates. Depending on the infrared absorption frequency range, spectrum data produced by FTIR analysis may be utilized to identify the particular chemical groups contained in the sample. For the mid-IR region, high spectral resolution data is typically obtained between 5000 and 400 cm^{-1}, kept between 10,000 and 4000 cm^{-1} for the near-IR area, [71].

These are the key components of an FTIR spectrometer:

1. IR-source
2. Beam splitter
3. Fixed and movable mirror
4. Sample cell
5. IR-Detector

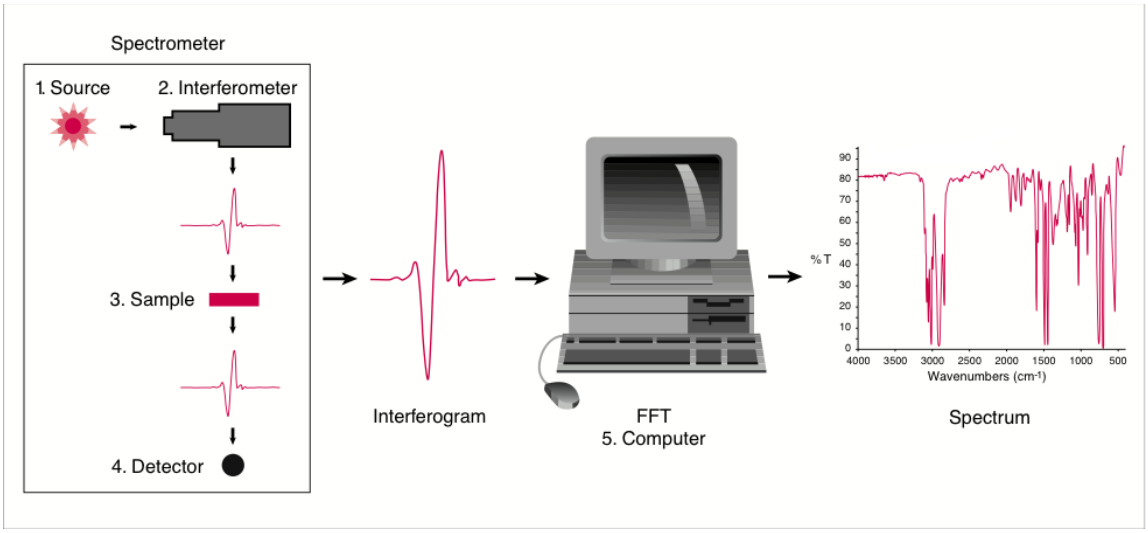

Figure 9: Illustration of FTIR components [72]

An interferometer, which contains an IR-source, splitter, two fixed mirrors, a laser, and an IR-detector, are the main piece of FTIR equipment. The beam splitter divides the energy from the source into two identical halves. A moving mirror receives one half, and a stationary mirror receives the other. A calibrating laser directs the movement of the moving mirror, which moves consistently back and forth. The beam splitter combines the reflected beams from the two mirrors before sending them via the sample compartment and, if present, the sample where absorption takes place, and finally to the detector. Lastly, a signal spectrum is created using the FT function [72].

An FTIR spectrometer (Perkin Elmer -100 FTIR) was used for the FTIR analysis. The study was carried out in the 4000-400 cm^{-1} wave range. By cutting out pieces that were the right size and matched the sample cell of the spectrometer, the pure PDMS and mixed matrix membranes could be examined. After being exposed to IR light, the spectra of the membrane samples were being used to determine the various bonds and different functional groups presence.

3.4.3 Scanning Electron Microscopy

The scanning electron microscope (SEM) generates numerous signals on the surface of solid objects using a focused stream of high-energy electrons. These signals basically produced by the intense interactions between electron-samples that reveal details on the

material's exterior morphology (texture), chemical make-up, crystalline structure, and elemental orientation. Choosing a specific area of the sample's surface to collect data and emphasise any spatial changes in these features is frequently used to produce a 2-dimensional picture [73].

Using a scanning mode, the common scanning electron microscopy (SEM) methods may take pictures of areas at various widths usually ranging from 1 cm to 5 microns. This permits magnifications of 20X to around 30,000X with a 50–100 nm spatial resolution. A specific point location on the sample may be examined using the SEM; this technique is particularly useful for figuring out chemical compositions in a qualitative or semi-quantitative way (using EDS).

The key elements of the SEM are [73]:

- Electron Source ("Gun")
- Electron Lenses
- Sample Stage
- Detectors
- Display / Data output devices

SEMs come with a variety of detectors, generally at least one of which is a secondary electron detector. The types of detectors that an instrument can support greatly affect its capabilities.

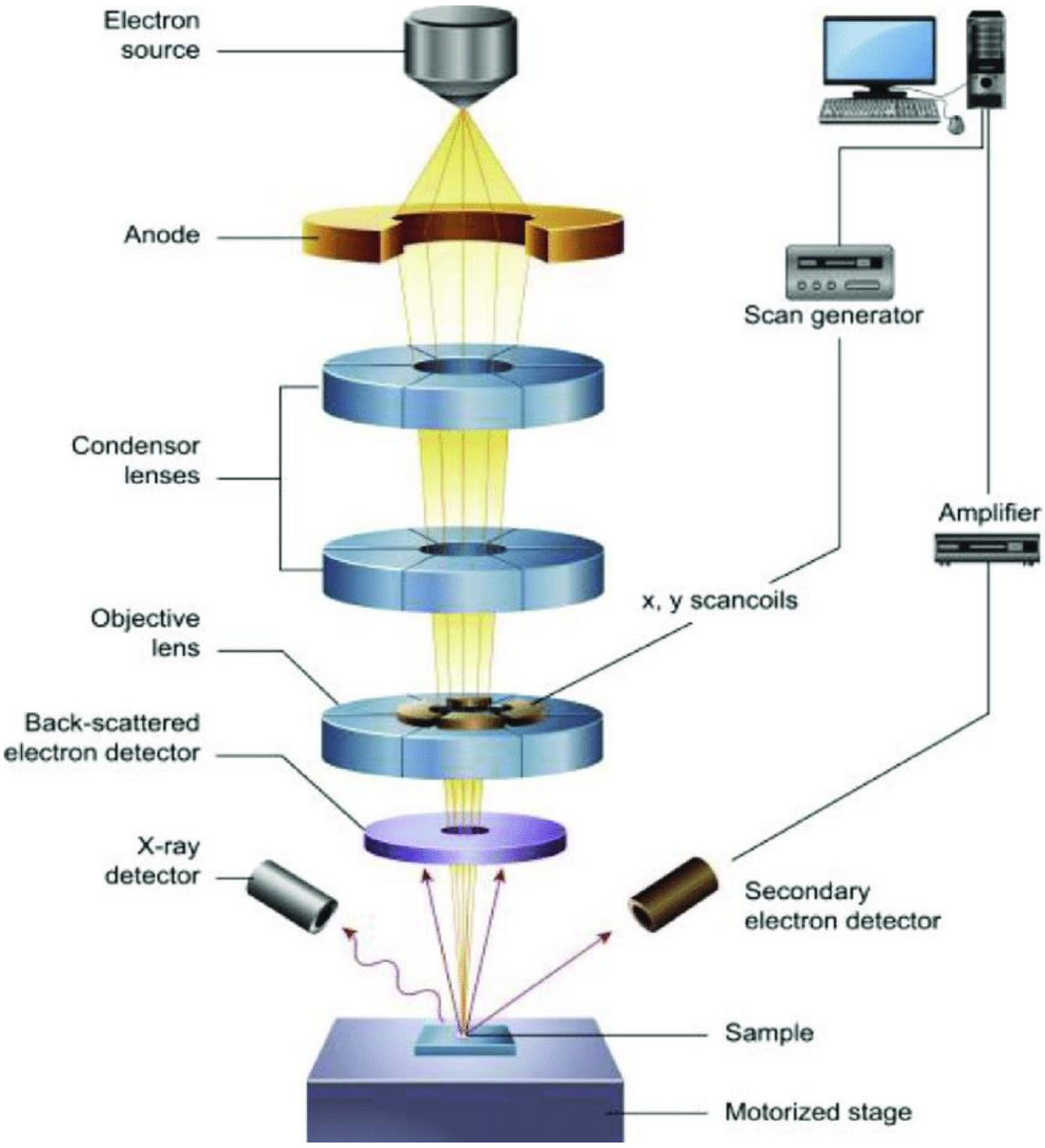

Figure 10: Schematic representation of SEM [74]

using the S-4700 electron microscope from Hitachi, Japan, for the SEM examination, and the JFC-1500 ion sputtering apparatus from JEOL Ltd. for the gold sputtering. Pictures were captured at resolutions ranging from 1000x to 10,000x at voltages generally between 5 kV and 10 kV. Pure modified membranes' surface and cross-section might be examined under these circumstances. The membranes were put atop the metal material and then broken with liquid nitrogen to create the cross-sectional pictures.

3.4.4 Universal Testing Machine (UTM)

UTM pulls on a material until it breaks in order to evaluate its tensile strength and behavior [75].

Tensile tests are performed on materials to forecast how they will respond to tension stresses. A straightforward tensile test shows the material's maximal tensile strength by pulling a sample until it breaks. During the test, the elongation of the sample and the amount of force applied to it are both assessed. A material's behavior is described using strain, which is the percentage change in length, and stress, which is the force per unit area. In contrast to strain, which is calculated by dividing the length change by the sample's initial length (L/L), stress is determined by dividing the force values by the cross-sectional area of the sample (F/A). A stress-strain curve, an XY graph used to depict the data, is then created [76].

A load cell, crosshead, extensometer, specimen grips, electronics, and a motor system are typical components of a UTM equipment. The equipment is run by software testing that records test parameters in accordance with recognized standards like ASTM and ISO and sets equipment safety parameters. During the test, the specimen's length and force are calculated and recorded. Designers and manufacturers may predict how a material will perform in its proposed use by measuring the force (F) necessary to stretch or extend a sample until it breaks or experiences irreversible deformation [76].

Figure 11: Schematic view of UTM [77]

The tensile strength of pure and hybrid membranes was assessed using a precision ultimate tensile tester from the SHIMADZU AGS-X series having a full 20 kN load. Each membrane sample was divided into 02 pieces according to the ASTM standard D882. Lastly, to perform the test using this standard, the stress-strain behavior was investigated [77].

3.4.5 Gas Permeation Testing

A single piece of gas permeation equipment was used to measure the permeability of gases across membranes. Permeability is the term used to describe a fluid's capacity to pass through a certain semi-permeable material. The given formula is being used to mathematically represent the permeability.

$$\frac{P_i}{\Delta l} = \frac{Q_i}{A\Delta p} \quad (3)$$

In this case, Pi stands for the permeability of gases, which is determined in Barrers (1 Barrer = 10 -10 cm3 (STP) cm/cm^2 s cm Hg). The membrane's active area (A) is 2 cm^2. Qi is the volumetric flow rate (cm3 (STP)/s) of permeate gas across an active membrane area with a surface area of 8 cm^2. L is the total membrane's thickness in centimeters. The pressure differential represented by the symbol p (cmhg) [78]. A simple formula, Eq., can be used to compute the ideal selectivity of the two gases.

$$\alpha \frac{1}{2} = \frac{\mathrm{P1}}{\mathrm{P2}} \quad (4)$$

Gas permeation composed of stainless-steel grade 316 is used for single gas permeation measurements. This gadget was built and installed by PHILOS. The equipment's flow diagram is given below. All the fabricated samples are put to the test at constant room temperature at various pressures of 2, 3, 4, and 5 Bar. The N_2, O_2, and CO_2 penetration rates were determined by placing the MMMs in a rig holder and supporting them with a porous ceramic disc. The feed gas stream is injected at the top of the cell, while permeate is passed from the bottom. A bubble flow meter is then used to manually determine the permeability. This configuration was used to calculate the single gas permeability and selectivity at various pressures.

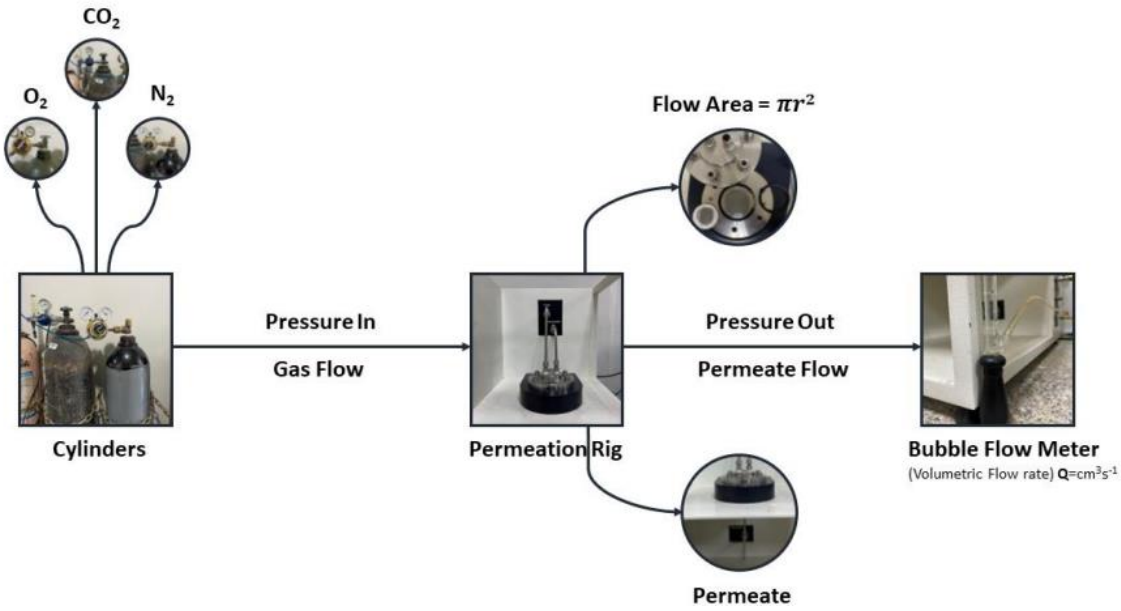

Figure 12: Single gas permeation testing process

Chapter 4

Results and Discussion

4.1 Characterization techniques

Membranes various characteristics have been examined by a various characterisation techniques. The following are the many methods used for characterization:

- FT-IR Spectroscopy, used to analyse the presence of various functional groups within the membrane structure
- XRD, used to check the crystaline and amorphous peaks and their intensity in a membrane samples
- SEM, used to evaluate and analyse the surface and cross morphology, and pore characteristics of the membrane
- EDX, used for mapping of specific elements (Cu, Ni) in a fabricated membrane sample
- UTS, used to determine the membranes' mechanical strength at a specific elongation rate

4.1.1 FT-IR Spectroscopy Analysis

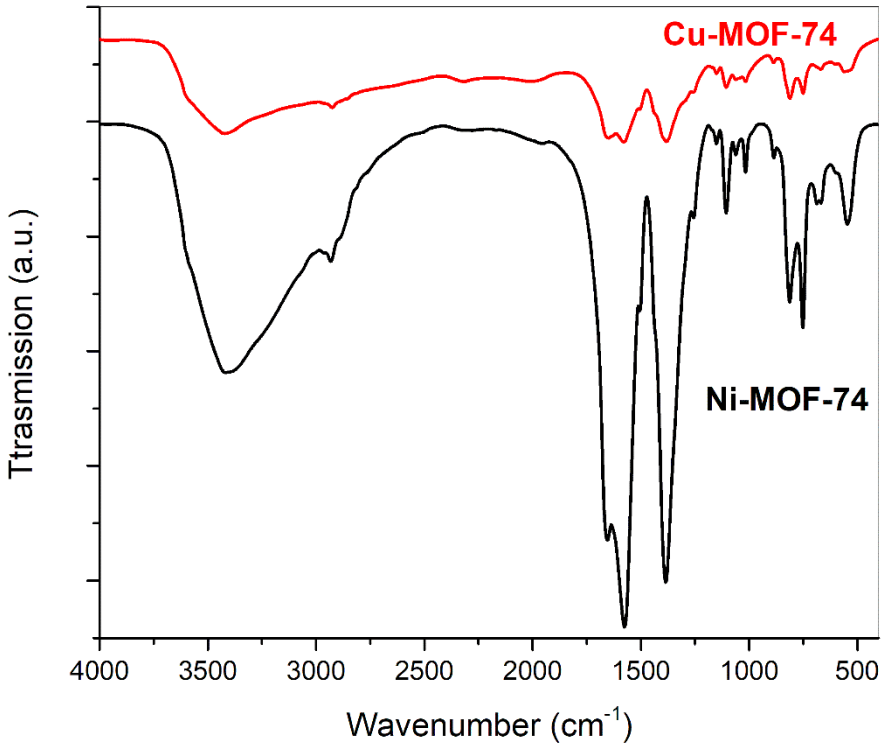

Figure 13: FTIR analysis of pure Cu-MOF-74 and Pure Ni-MOF-74.

The examination of the FTIR spectra for pure Cu and Ni-MOF-74, and all the manufactured membranes is shown in Figure 13. It shows the presence of different functional groups in these samples. As may be observed in Figure (13) C=O and C-C=O Stretching vibrations, which depict how Ni-MOF nanoparticles were created. Also, the Ni-MOF-74 stretching vibrations of the uncoordinated hydroxy group (-OH) were confirmed by the faint wide peaks between 2800 and 3600 cm^{-1}, which matched the findings from the literature [58]. The C-H and C-O stretching vibrations are represented by distinctive peaks at 730 cm^{-1} and a band at 1112 cm^{-1}, respectively, in the FTIR spectra for the Cu-MOF [79, 80] Whereas the asymmetric and symmetric stretching of carboxylate groups are shown, respectively, at 1647 cm^{-1} and 1373 cm^{-1} [81]. The crystallinity of Cu and Ni-MOF nanoparticles is therefore well illustrated by these data.

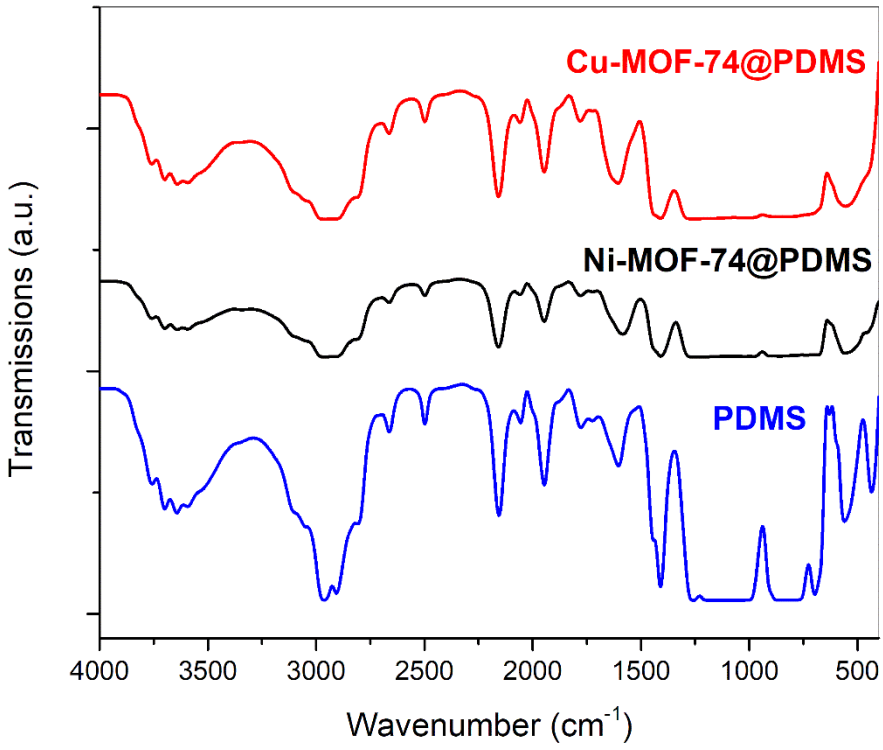

Figure 14: FTIR analysis of Pristine PDMS membrane, Ni-MOF-74@PDMS and Cu-MOF-74@PDMS

Figure (14) showing the FTIR spectra of pristine rubbery PDMS membrane and MMMs. As seen in the pristine PDMS membrane spectrum there are energetic adsorption bands at 805 cm^{-1} [82], 1024 cm^{-1} [83], 1258 cm^{-1} [82], and 2960 cm^{-1} [84] assigning the Si–C–H, Si–O–Si, Si–C, and C–H of the $–CH_3$ groups bonds, respectively. demonstrating the MMMs' appropriate fabrication by contrasting their spectra with those of pure PDMS.

4.1.2 X-ray Diffraction (XRD)

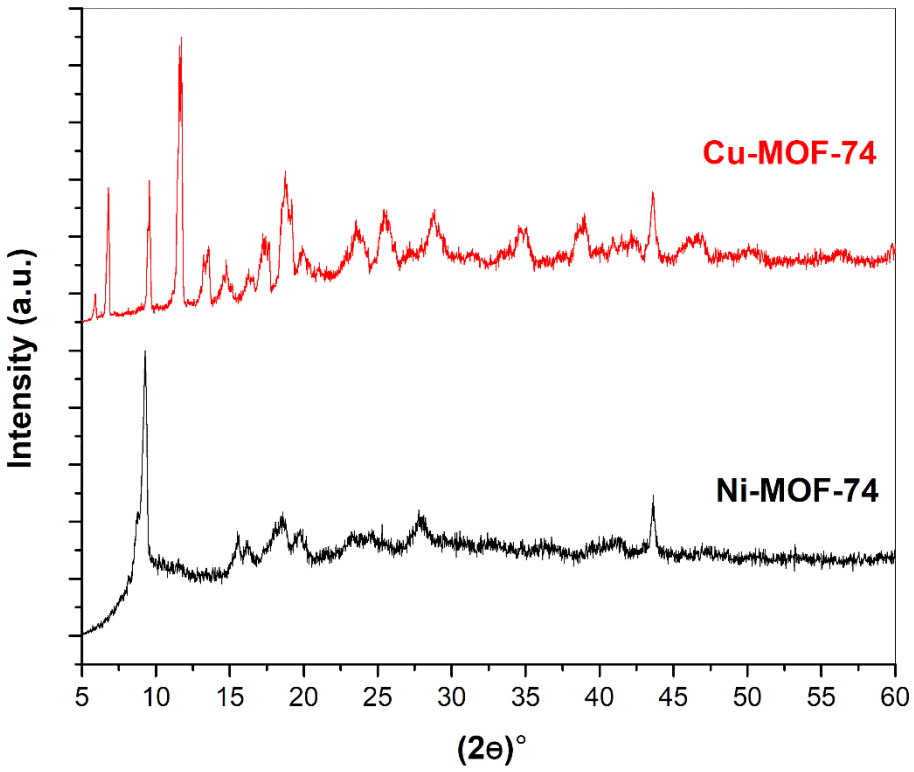

Figure 15: XRD analysis of Pure Cu-MOF-74 and Pure Ni-MOF-74.

The XRD patterns of pure Ni-MOF-74, Cu-MOF-74, virgin PDMS membrane, and MMMs employing MOFs are shown in Figures 15 and 16. The crystalline structure was confirmed by the powder XRD patterns of pure Ni and Cu MOF nanoparticles (figure). The (1 2 0) crystallographic plane can be detected in the Ni-MOF nanoparticles as a strong peak at 7° [58] and the Cu-MOF nanoparticles' diffraction peaks similarly match what has been described in the literature [85, 86].

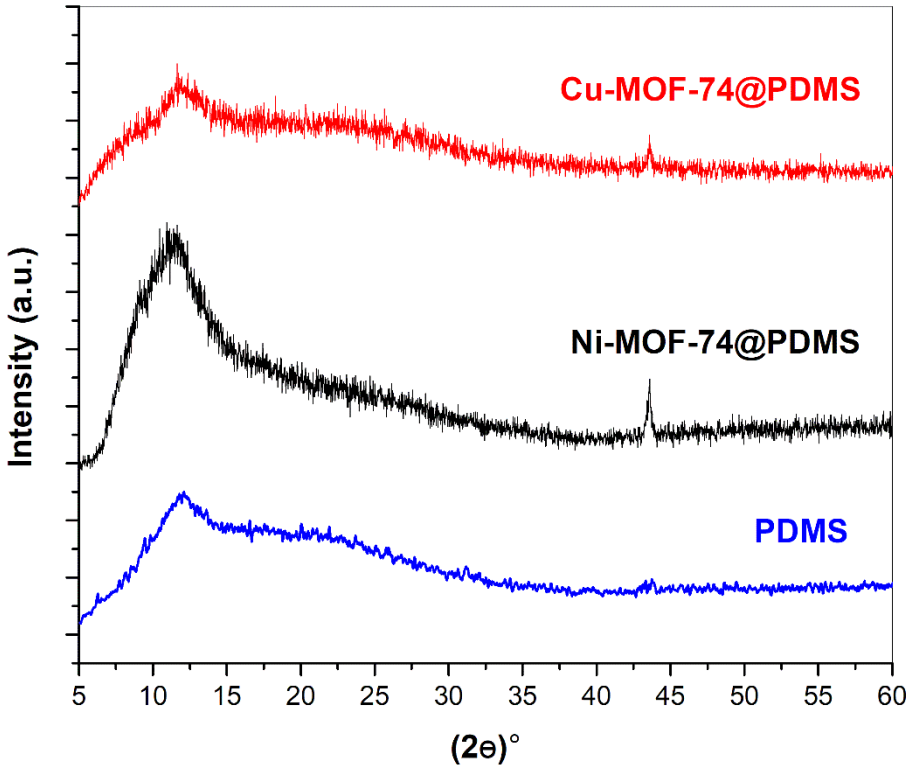

Figure 16: XRD analysis of Pristine PDMS membrane, Ni-MOF-74@PDMS and Cu-MOF-74@PDMS

Figure (8B) shows the pure PDMS indicating its amorphous structure through broad peaks around 12 and 22.5 [35, 87] and the Ni and Cu-MOF@PDMS exhibit a very similar XRD pattern to the pure PDMS, which has weak peaks that support the patterns of Ni and Cu MOFs, respectively. Furthermore, according to the XRD examination, the addition of Ni and Cu MOFs to PDMS does not enough alter its amorphous structure and keep the effective behavior [88].

4.1.3 Scanning Electron Microscopy (SEM)

SEM was used to analyse the morphology of all the materials, including pure PDMS membrane, pure Cu and Ni MOFs, and all the MOFs containing MMMs (20000x, 15000x, 10000x, 5000x, 2500x, 1000x, and 500x). The SEM pictures of pure Ni-MOF-74, Cu-MOF-74 with particles between 20 and 30 nm, and virgin PDMS membrane's surface and cross section morphology images are shown in Figure (17). Figures (18) and (19) show surface and cross-section photos of all MMMs made with Ni-MOF and Cu-MOF at different concentrations of 0.5, 1, 1.5, and 2 wt%, respectively. All of the photos exhibit a flawlessly dense structure with no discernible signs of any interfacial gaps, indicating good compatibility in between MOF nanoparticles and the PDMS matrix. While increasing the amount of MOF causes the agglomeration of particles within the polymer matrix, results in the formation of voids known as nano gaps and is justified by an increase in the permeation rate. The SEM analysis is carried out after the gas permeation testing of each membrane sample. Due to the polymer chains' inability to properly pack together, small voids develop [57, 89]. The results of the membrane's ultimate tensile strength further demonstrate that adding filler decreases the membrane's tensile strength because of agglomeration.

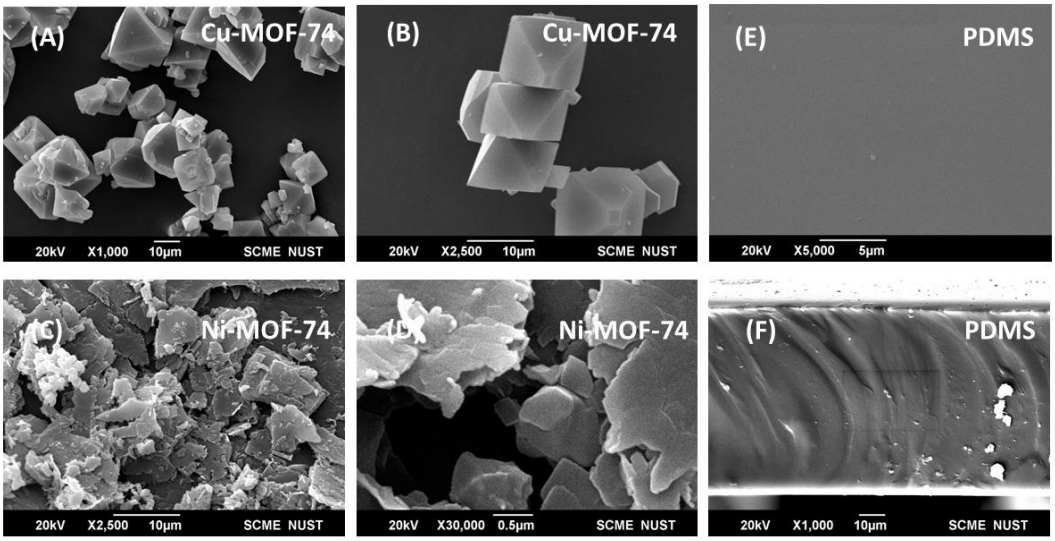

Figure 17: SEM images of (A, B) Pure Cu-MOF-74, (C, D) Pure Ni-MOF-74. (E, F) Pristine PDMS membrane's surface and cross sections images, respectively.

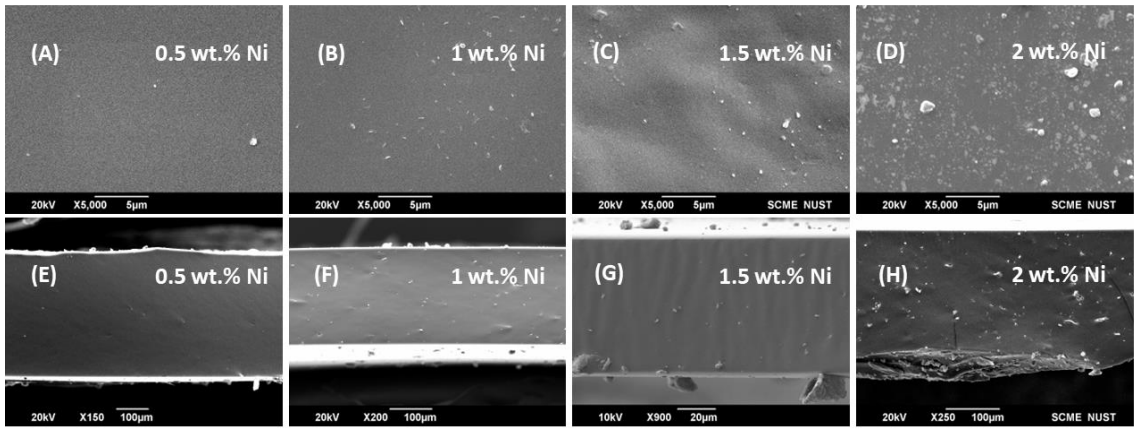

Figure 18: SEM images of (A, B, C, D) Surface of 0.5wt% Ni-MOF@PDMS, 1wt% Ni-MOF@PDMS, 1.5wt% Ni-MOF@PDMS, 2wt% Ni-MOF@PDMS. (E, F, G, H) Cross section of 0.5wt% Ni-MOF@PDMS, 1wt% Ni-MOF@PDMS, 1.5wt% Ni-MOF@PDMS, 2wt% Ni-MOF@PDMS

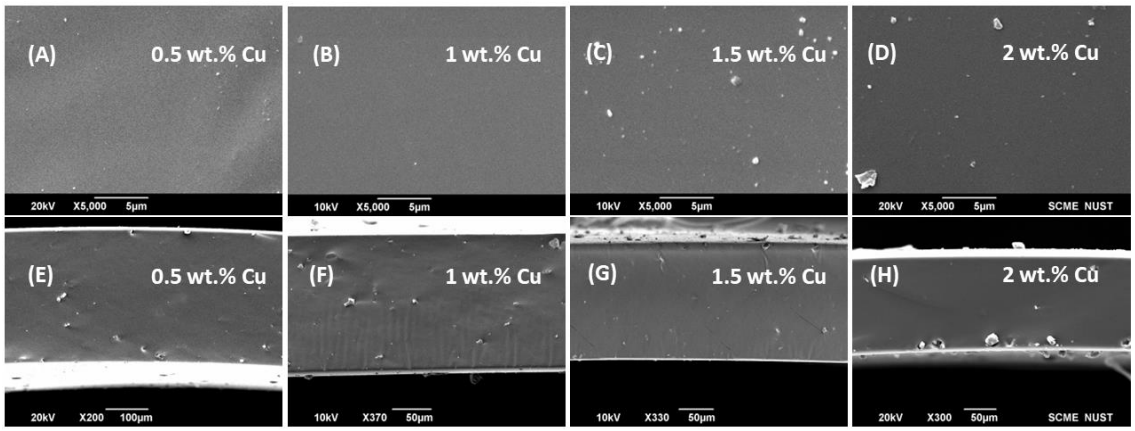

Figure 19: SEM images of (A, B, C, D) Surface of 0.5wt% Cu-MOF@PDMS, 1wt% Cu-MOF@PDMS, 1.5wt% Cu-MOF@PDMS, 2wt% Cu-MOF@PDMS. (E, F, G, H) Cross section of 0.5wt% Cu-MOF@PDMS, 1wt% Cu-MOF@PDMS, 1.5wt% Cu-MOF@PDMS, 2wt% Cu-MOF@PDMS

4.1.4 Energy-dispersive X-ray spectroscopy (EDX)

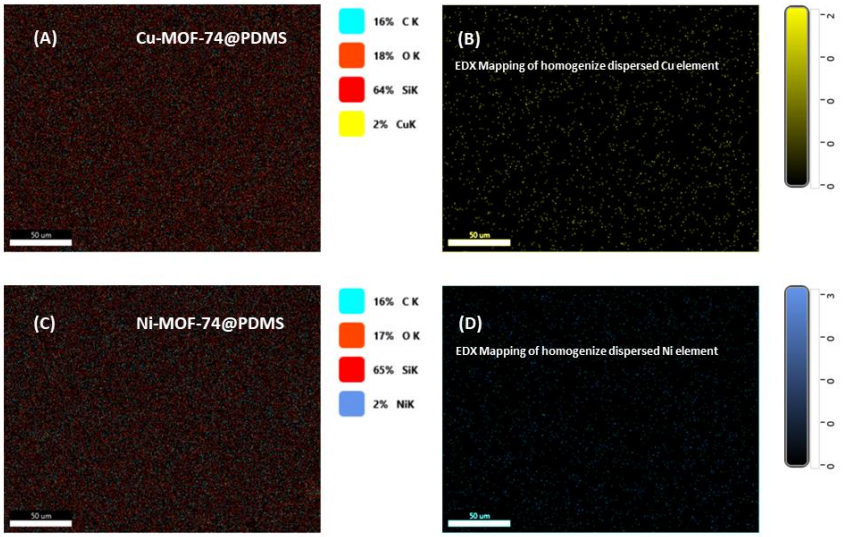

Figure 20: EDX mapping of (A, B) Cu in Cu-MOF-74@DPMS MMM. (C, D) Ni in Ni-MOF-74@DPMS MMM.

Figure (20) shows EDX mapping spectroscopy verifying the uniform dispersion of MOF nanofillers within the matrix (PDMS). Due to the presence of Cu or Ni elements in the

PDMS matrix, EDX mapping was used to verify the homogeneous distribution of Cu and Ni elements and the uniform dispersion of Cu-MOF and Ni-MOF, respectively, inside the polymer matrix.

4.1.5 Ultimate Tensile Strength (UTS)

The UTS of pure rubbery PDMS membrane and all MMMs incorporating MOFs are shown in Figure (21). UTS measured at a 0.5mm/min optimal elongation rate. Following several runs, the elongations rate is calculated. To accurately evaluate the strength of membrane samples, it must be optimized—neither too low nor too high. The testing is conducted throughout at a modest elongation rate of 0.5mm/min. As seen in figure (10), adding little quantities of MOFs (Cu, Ni) at 0.5 and 1 weight percent increases the tensile strength to a high value. Nevertheless, the tensile strength decreased to even lower levels than the value of a pure PDMS membrane with 0wt% filler when the amount of Filler was raised above 1wt%. According to the research [90], the disruption of stiffness at the polymer/filler interface is what causes the strength of MMM to decrease as filler loading increases. As the region around filler is more stiff than the polymer matrix, increasing the filler loading causes the interface to become less stiff, which leads to the development and spread of cracks [91].

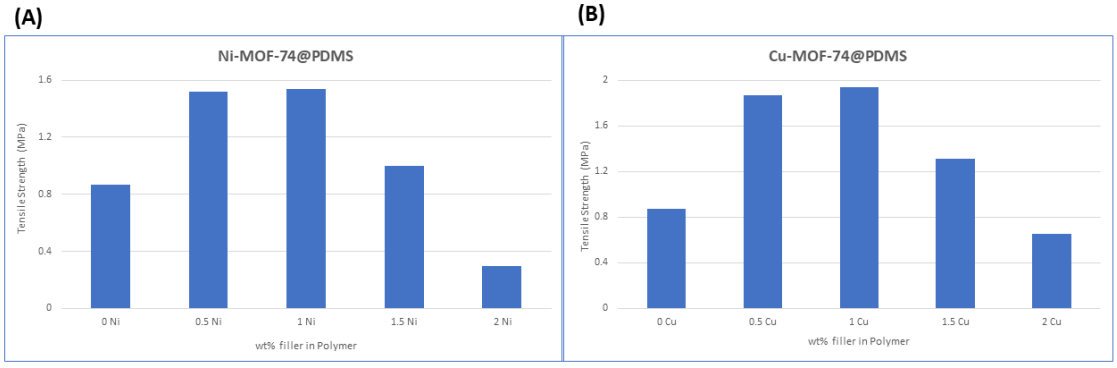

Figure 21: Mechanical Strength analysis of (A) Ni-MOF-74@PDMS containing 0, 0.5, 1, 1.5, 2wt% filler (B) Cu-MOF-74@PDMS containing 0, 0.5, 1, 1.5, 2wt% filler

4.2 Gas Transport Analysis

A single gas (CO_2, O_2, N_2) permeation via a stainless-steel permeation rig is evaluated on the pristine PDMS membrane and all of the manufactured MMMs comprising 0.5wt%, 1wt%, 1.5wt%, and 2wt% Ni and Cu-MOF-74 at pressure ranges of 2, 3, 4, and 5 Bars. The findings of all membranes' single gas permeation, as well as their selectivity at all subsequent pressures, are shown in Figures (22), and (23). The figures show that the permeability and selectivity are at their highest at 2 Bar. Due to CO_2's maximum adsorption at low pressure, selectivity will be high.

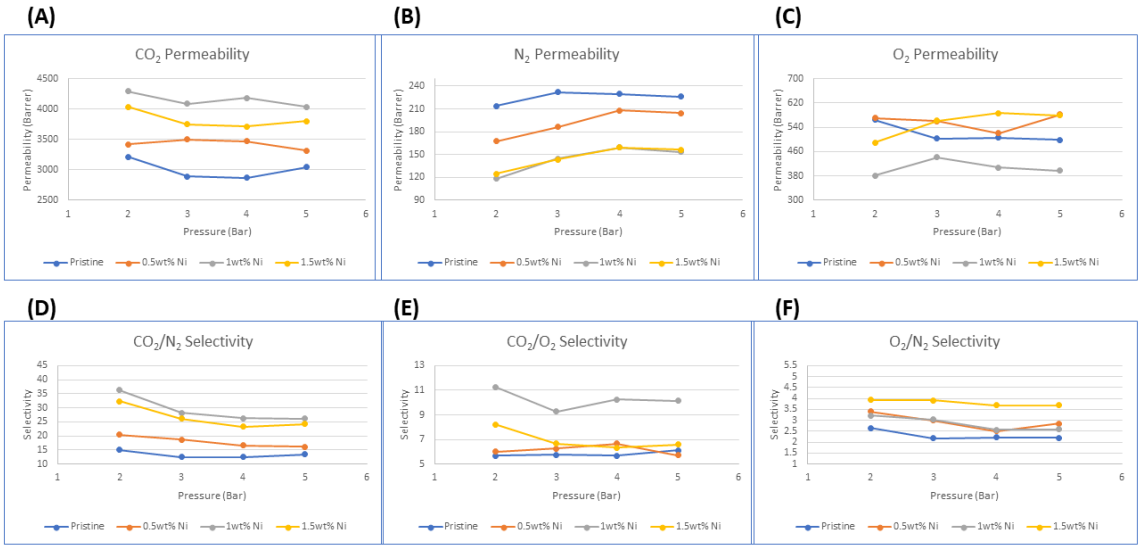

Figure 22: Pure PDMS and MMMs having 0.5wt%, 1wt%, 1.5wt% Ni-MOF-74, gas permeability of (A) CO_2, (B) N_2, (C) O_2 and gas selectivity of (D) CO_2/N_2, (E) CO_2/O_2, (F) O_2/N_2.

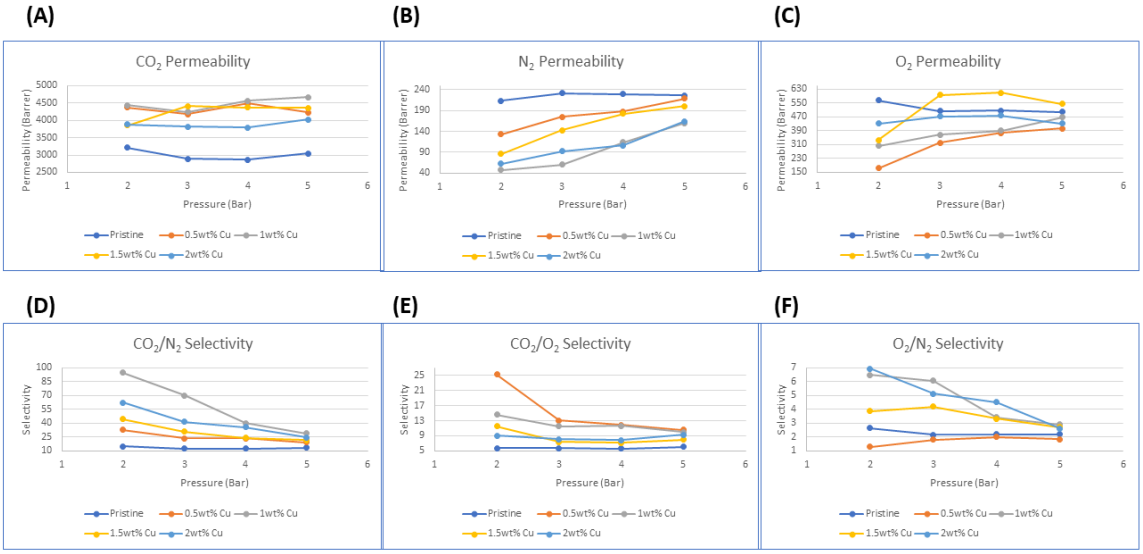

Figure 23: Pure PDMS and MMMs having 0.5wt%, 1wt%, 1.5wt%, 2wt% Cu-MOF-74, gas permeability of (A) CO_2, (B) N_2, (C) O_2 and gas selectivity of (D) CO_2/N_2, (E) CO_2/O_2, (F) O_2/N_2.

The best Ni-MOF and Cu-MOF findings for all the gases at 2 Bar are displayed in Figure (24), and Table (11). The disruption in polymer chain packing, which results in the production of nanogaps or voids, which increases the diffusion channel for the gas transport, is what causes the permeation trend to increase when filler loading into the polymer matrix. In comparison to published figures, the permeability of the pure rubbery PDMS membrane for CO_2 is 3212 Barrer [34, 67]. The best permeation findings for CO_2 are at 1wt% Ni-MOF and Cu-MOF, which are 4288 and 4432 Barrer, respectively, representing increases of 34% for Ni-MOF and 40% for Cu-MOF. The permeation for CO_2 is increasing with the quantity of filler whereas it is dropping for N_2. The virgin PDMS membrane's selectivity for CO_2/N_2 and O_2/N_2 is 16 and 2.64, respectively. While the CO_2/N_2 and O_2/N_2 selectivity rose to 36.2 and 3.2 for 1wt% Ni-MOF@PDMS, which is an increase of 125% for CO_2/N_2 and 25% for O_2/N_2, it climbed to 94.7 and 6.47 for 1wt% Cu-MOF@PDMS, which is an increase of 482% for CO_2/N_2 and 150% for O_2/N_2. Consequently, the Lewis acidic sites of MOF-74-NCs for CO_2 and O_2 as well as the presence of porous fillers are both responsible for this increased selectivity [56]. Changes

in metal type improved CO_2 adsorption in low-pressure areas. This suggests that these open metal sites are the primary sites to adsorb at low pressures, and that raising the metal ion's Lewis acidity improved the loving affinity of CO_2 toward MOF-74. The Lewis acidity of the metal cations was measured by looking at the alterations in the vibrational peak brought on by the acetone C=O bond connected to the open metal site. This discovery demonstrates a clear correlation between a metal cation's ability to bind CO_2 and its Lewis acidity [28].

Table 11: comparing the gas (CO_2) separation efficiency and CO_2/N_2 selectivity of this research with the other literature

Membrane	**Permeability (Barrer)**			**Ideal Selectivity**		
	CO_2 **(±44)**	O_2 **(±21)**	N_2 **(±12)**	CO_2/N_2	CO_2/O_2	O_2/N_2
PDMS	3212	565	214	15	5.68	2.64
0.5wt%Ni-MOF-74@PDMS	3418.108	569.68	167.55	20.4	6	3.4
1wt%Ni-MOF-74@PDMS	4288.04	381.15	118.29	36.25	11.25	3.22
1.5wt%Ni-MOF-74@PDMS	4035.80	490.06	124.74	32.35	8.23	3.92
0.5wt%Cu-MOF-74@PDMS	4367.77	172.89	132.78	32.89	25.26	1.30
1wt%Cu-MOF-74@PDMS	4432.64	302.95	46.78	94.73	14.63	6.47
1.5wt%Cu-MOF-74@PDMS	3850.06	335.20	86.37	44.57	11.48	3.88
2wt%Cu-MOF-74@PDMS	3885.77	431.75	62.17	62.5	9	6.94

Due to the filler's uniform distribution throughout the polymer matrix, the Cu MOF produces superior outcomes than the Ni MOF. The Cu MOF is displaying a superior morphology than Ni MOF, as can be seen in the aforementioned SEM photos. The agglomeration of filler particles into the matrix and creation of nonselective gaps, which provides additional diffusion channel for N_2 as well, cause the selectivity for both MOFs to decrease when we raise the filler quantity over 1wt%. The MMM of 2wt% Ni-MOF@PDMS was so fragile and weak that it was never even constructed. Due to its tensile strength, which is described above, MMM over 1wt% is neither an efficient nor a selective membrane. Nevertheless, the poor CO_2/N_2 selectivity of 32.3 was caused by the additional 1.5 wt% filler added to the polymer matrix. The thickness of each membrane is approximately 180 to 200 um.

Hence, based on gas transport tests (high permeability for CO_2, and O_2, and low for N_2, and good CO_2/N_2 and O_2/N_2 selectivity), 1wt% Ni-MOF-74@PDMS and Cu-MOF-74@PDMS were chosen as the best MMMs and Ni—OH MOF-74's group, Lewis acidic sites, open metal sites that draw in CO_2 and O_2 ($CO_2>O_2$), SEM images (verified by structural morphology of membranes as well as their SEM-EDX mapping of Ni and Cu element within the polymer matrix), and UTS results analysis all contribute to this (Highest Ultimate tensile strength comparative to other MMMs and pristine rubbery PDMS membrane). As previously said, the MOF modification is the next strategy, which entails thermally annealing MOFs with amine-based ligands to enhance the performance of fabricated membranes for separating gases and the results of their permeation.

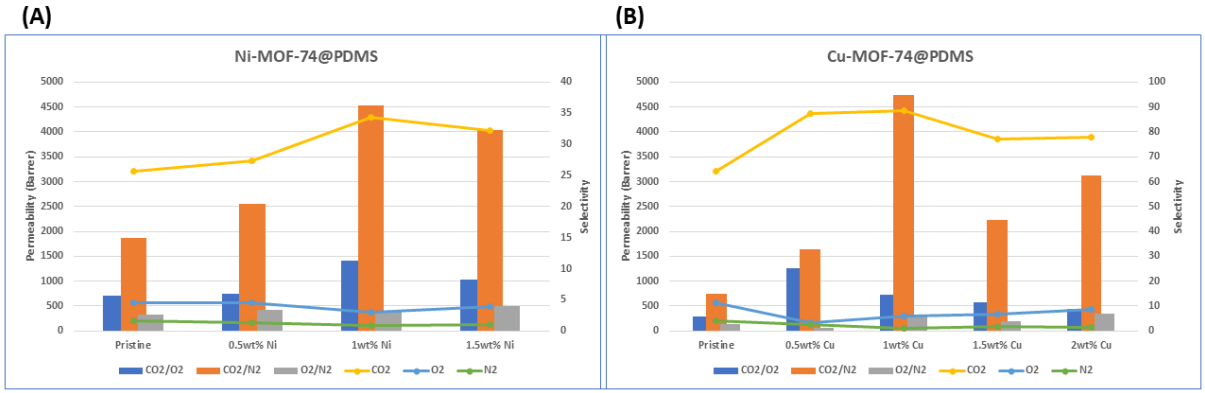

Figure 24: CO_2, O_2, and N_2 permeability (Barrer) and CO_2/N_2, CO_2/O_2, O_2/N_2 ideal selectivity of Pure PDMS and MMMs having 0.5wt%, 1wt%, 1.5wt%, 2wt% of (A) Ni-MOF-74, (B) Cu-MOF-74 at 2 Bar.

Conclusion

We described how to make pure rubbery PDMS membranes and all of the manufactured MMMs by using Ni and Cu-MOF-74 with 0.5, 1, 1.5, and 2 weight percent filler into the PDMS polymer matrix. All of the membrane samples were examined using a stainless-steel permeation apparatus with a single gas permeation of CO_2, O_2, and N_2 (>99% purity) at successive pressures of 2, 3, 4, and 5 Bar. The surface and cross morphology of all the MMMs were investigated by SEM images, and all the samples underwent XRD analysis in order to examine the crystallinity behavior of Ni and Cu-MOF-74, as well as the amorphous behavior of pure PDMS membranes and the mix behavior of MMM samples. After that the FTIR analysis was conducted to examine the functional group within the polymer matrix and MOFs, and Ultima was used to test the membrane samples After conducting several tests, it has been determined that the 1wt%Ni-MOF-74@PDMS and 1wt%Cu-MOF-74@PDMS are the most effective mixed matrix membranes (MMMs) for low pressure applications of up to 2 Bar. This decision was based on various factors such as the homogenous dispersion of the MOFs within the polymer matrix, as verified through SEM-EDX mapping of the Ni and Cu elements within the polymer matrix. In addition, these MMMs demonstrated high mechanical strength at the 1wt% concentration. Furthermore, these MMMs exhibited a significant increase in CO_2 permeation, with the Ni-MOF membrane increasing to 4288 Barrer (a 34% increase) and the Cu-MOF membrane increasing to 4432 Barrer (a 40% increase). These results suggest that the 1wt%Ni-MOF-74@PDMS and 1wt%Cu-MOF-74@PDMS are promising options for low-pressure CO_2 separation applications due to their excellent performance in terms of homogeneity, mechanical strength, and permeability. The selectivity for CO_2/N_2 and O_2/N_2 in pure PDMS membranes is 16 and 2.64, respectively. While the CO_2/N_2 and O_2/N_2 selectivity rose by 125% for 1wt% Ni-MOF@PDMS and by 25% for 1wt% Cu-MOF@PDMS, respectively, to 36.2 and 3.2, respectively, the selectivity increased by 482% for 1wt% Ni-MOF@PDMS and by 150% for 1wt% Cu-MOF@PDMS. The MOF-74-NCs's Lewis acidic sites for CO_2 and O_2, as well as the inclusion of porous fillers, are the two factors that contribute to this increased selectivity. The weak M-N (M=Cu, Ni)

bond can be broken to expand unpaired electrons on the N atoms to adsorb CO_2, but there may also be a method to increase the MOF dependence on CO_2 gas and increase the diffusion path for CO_2 transport. Additionally, a thick porous support layer can be created to further increase the mechanical strength of the membrane. We concluded by demonstrating the significant potential of these MMMs, which include Ni and Cu-MOF nanocrystals into the rubbery PDMS polymer matrix, to reduce CO_2 emissions sustainably and to aid in the gas separation process.

References:

[1]. By fuel type-Exajoules, C. and C.D. Emissions, *bp Statistical Review of World Energy June 2020.* 2006.

[2]. Goldstein, A., et al., *Protecting irrecoverable carbon in Earth's ecosystems.* 2020. **10**(4): p. 287-295.

[3]. Liguori, S., et al., *Opportunities and challenges of low-carbon hydrogen via metallic membranes.* 2020. **80**: p. 100851.

[4]. Sazali, N.J.I.J.o.H.E., *Emerging technologies by hydrogen: A review.* 2020. **45**(38): p. 18753-18771.

[5]. Muradov, N.Z. and T.N.J.I.j.o.h.e. Veziroğlu, *"Green" path from fossil-based to hydrogen economy: an overview of carbon-neutral technologies.* 2008. **33**(23): p. 6804-6839.

[6]. Liang, F.-Y., et al., *The role of natural gas as a primary fuel in the near future, including comparisons of acquisition, transmission and waste handling costs of as with competitive alternatives.* 2012. **6**(1): p. 1-24.

[7]. Wasiu, A.B. and M.R. Heikal, *The effect of carbon dioxide content-natural gas on the performance characteristics of engines: a review.* 2012.

[8]. Darmstadter, J., *Energy and population*. 2004: Resources for the Future Washington.

[9]. York, R.J.S.s.r., *Demographic trends and energy consumption in European Union Nations, 1960–2025.* 2007. **36**(3): p. 855-872.

[10]. Owen, N.A., O.R. Inderwildi, and D.A.J.E.p. King, *The status of conventional world oil reserves—Hype or cause for concern?* 2010. **38**(8): p. 4743-4749.

[11]. Baker, R.W.J.I. and e.c. research, *Future directions of membrane gas separation technology.* 2002. **41**(6): p. 1393-1411.

[12]. Aaron, D., C.J.S.s. Tsouris, and technology, *Separation of* CO_2 *from flue gas: a review.* 2005. **40**(1-3): p. 321-348.

[13]. Yu, C.-H., et al., *A review of* CO_2 *capture by absorption and adsorption.* 2012. **12**(5): p. 745-769.

[14]. Relvas, F., et al., *Single-stage pressure swing adsorption for producing fuel cell grade hydrogen.* 2018. **57**(14): p. 5106-5118.

[15]. Ye, F., et al., *Artificial neural network based optimization for hydrogen purification performance of pressure swing adsorption.* 2019. **44**(11): p. 5334-5344.

[16]. Fakhroleslam, M., R.B. Boozarjomehry, and S.J.I.J.o.H.E. Fatemi, *Design of a dynamical hybrid observer for pressure swing adsorption processes.* 2017. **42**(33): p. 21027-21039.

[17]. Yousef, A.M., et al., *New approach for biogas purification using cryogenic separation and distillation process for* CO_2 *capture.* 2018. **156**: p. 328-351.

[18]. Bernardo, G., et al., *Recent advances in membrane technologies for hydrogen purification.* 2020. **45**(12): p. 7313-7338.

[19]. Sołowski, G., et al., *Production of hydrogen from biomass and its separation using membrane technology.* 2018. **82**: p. 3152-3167.

[20]. Yin, H. and A.C.J.C. Yip, *A review on the production and purification of biomass-derived hydrogen using emerging membrane technologies.* 2017. **7**(10): p. 297.

[21]. Chung, T.-S., et al., *Mixed matrix membranes (MMMs) comprising organic polymers with dispersed inorganic fillers for gas separation.* 2007. **32**(4): p. 483-507.

[22]. Bastani, D., et al., *Polymeric mixed matrix membranes containing zeolites as a filler for gas separation applications: A review.* 2013. **19**(2): p. 375-393.

[23]. Zornoza, B., et al., *Metal organic framework based mixed matrix membranes: An increasingly important field of research with a large application potential.* 2013. **166**: p. 67-78.

[24]. Vu, D.Q., W.J. Koros, and S.J.J.J.o.m.s. Miller, *Mixed matrix membranes using carbon molecular sieves: I. Preparation and experimental results.* 2003. **211**(2): p. 311-334.

[25]. Wang, B., et al., *Applications of metal–organic frameworks for green energy and environment: New advances in adsorptive gas separation, storage and removal.* 2018. **3**(3): p. 191-228.

[26]. Khatua, S., et al., *Stable multiresponsive luminescent MOF for colorimetric detection of small molecules in selective and reversible manner.* 2015. **27**(15): p. 5349-5360.

[27]. Tibbetts, I. and G.E.J.M. Kostakis, *Recent bio-advances in metal-organic frameworks.* 2020. **25**(6): p. 1291.

[28]. Choe, J.H., H. Kim, and C.S.J.M.C.F. Hong, *MOF-74 type variants for CO 2 capture.* 2021. **5**(14): p. 5172-5185.

[29]. Zhang, Z., et al., *Improvement of* CO_2 *adsorption on ZIF-8 crystals modified by enhancing basicity of surface.* 2011. **66**(20): p. 4878-4888.

[30]. Sanaeepur, H., et al., *Cellulose acetate/nano-porous zeolite mixed matrix membrane for* CO_2 *separation.* 2015. **5**(3): p. 291-304.

[31]. Bushell, A.F., et al., *Gas permeation parameters of mixed matrix membranes based on the polymer of intrinsic microporosity PI*m^{-1} *and the zeolitic imidazolate framework ZIF-8.* 2013. **427**: p. 48-62.

[32]. Madaeni, S.S., et al., *Effect of coating method on gas separation by PDMS/PES membrane.* 2013. **53**(9): p. 1878-1885.

[33]. Fang, M., et al., *ZIF-8/PDMS mixed matrix membranes for propane/nitrogen mixture separation: Experimental result and permeation model validation.* 2015. **474**: p. 103-113.

[34]. Mansourpanah, Y., F.J.J.o.M.S. Bagri, and Research, *Improvement of the performance of PDMS top layer of mixed matrix membrane incorporated with treated ZIF-8 for gas separation.* 2021. **7**(2): p. 111-117.

[35]. Wang, X., et al., *ZIF-7/PDMS mixed matrix membranes for pervaporation recovery of butanol from aqueous solution.* 2016. **163**: p. 39-47.

[36]. Robeson, L.J.P.E. and Science, *Applications of polymer blends: Emphasis on recent advances.* 1984. **24**(8): p. 587-597.

[37]. Mannan, H.A., et al., *Recent applications of polymer blends in gas separation membranes.* 2013. **36**(11): p. 1838-1846.

[38]. Belmabkhout, Y. and A.J.A. Sayari, *Effect of pore expansion and amine functionalization of mesoporous silica on CO 2 adsorption over a wide range of conditions.* 2009. **15**: p. 318-328.

[39]. Liu, D. and C.J.J.o.M.C. Zhong, *Understanding gas separation in metal–organic frameworks using computer modeling.* 2010. **20**(46): p. 10308-10318.

[40]. Chen, Y. and J.J.C. Jiang, *A bio-metal–organic framework for highly selective* CO_2 *capture: A molecular simulation study.* 2010. **3**(8): p. 982-988.

[41]. Li, Y. and R.T.J.L. Yang, *Gas adsorption and storage in metal− organic framework MOF-177.* 2007. **23**(26): p. 12937-12944.

[42]. McDonald, T.M., et al., *Capture of carbon dioxide from air and flue gas in the alkylamine-appended metal–organic framework mmen-Mg2 (dobpdc).* 2012. **134**(16): p. 7056-7065.

[43]. Erucar, I., S.J.I. Keskin, and E.C. Research, *High* CO_2 *selectivity of an amine-functionalized metal organic framework in adsorption-based and membrane-based gas separations.* 2013. **52**(9): p. 3462-3472.

[44]. Seoane, B., et al., *Metal–organic framework based mixed matrix membranes: a solution for highly efficient CO 2 capture?* 2015. **44**(8): p. 2421-2454.

[45]. Basu, S., et al., *MOF-containing mixed-matrix membranes for* CO_2/CH_4 *and* CO_2/N_2 *binary gas mixture separations.* 2011. **81**(1): p. 31-40.

[46]. Perez, E.V., et al., *Mixed-matrix membranes containing MOF-5 for gas separations.* 2009. **328**(1-2): p. 165-173.

[47]. Zornoza, B., et al., *Functionalized flexible MOFs as fillers in mixed matrix membranes for highly selective separation of CO 2 from CH 4 at elevated pressures.* 2011. **47**(33): p. 9522-9524.

[48]. Crake, A., et al., CO_2 *capture and photocatalytic reduction using bifunctional* TiO_2*/MOF nanocomposites under UV–vis irradiation.* 2017. **210**: p. 131-140.

[49]. Li, T., et al., *Carbon dioxide selective mixed matrix composite membrane containing ZIF-7 nano-fillers.* 2013. **425**: p. 235-242.

[50]. Bux, H., et al., *Ethene/ethane separation by the MOF membrane ZIF-8: Molecular correlation of permeation, adsorption, diffusion.* 2011. **369**(1-2): p. 284-289.

[51]. Nordin, N.A.H.M., et al. *Modified ZIF-8 mixed matrix membrane for* CO_2/CH_4 *separation*. in *AIP Conference Proceedings*. 2017. AIP Publishing LLC.

[52]. Huang, A., et al., *Organosilica-functionalized zeolitic imidazolate framework ZIF-90 membrane with high gas-separation performance.* 2012. **51**(42): p. 10551-10555.

[53]. Bae, T.J.S., *Long JR Energy Environ.* 2013. **6**: p. 3565-3569.

[54]. Kim, H., et al., *Effective* CO_2 *and CO separation using [*m^2 *(DOBDC)](M= Mg, Co, Ni) with unsaturated metal sites and excavation of their adsorption sites.* 2019. **11**(7): p. 7014-7021.

[55]. Kwon, H.T. and H.-K.J.J.o.t.A.C.S. Jeong, *In situ synthesis of thin zeolitic–imidazolate framework ZIF-8 membranes exhibiting exceptionally high propylene/propane separation.* 2013. **135**(29): p. 10763-10768.

[56]. Mason, J.A., et al., *Evaluating metal–organic frameworks for post-combustion carbon dioxide capture via temperature swing adsorption.* 2011. **4**(8): p. 3030-3040.

[57]. Cong, H., et al., *Polymer–inorganic nanocomposite membranes for gas separation.* 2007. **55**(3): p. 281-291.

[58]. Liu, M., et al., *High-throughput* CO_2 *capture using PI*m^{-1}*@ MOF based thin film composite membranes.* 2020. **396**: p. 125328.

[59]. Gaikwad, S., et al., *Enhanced* CO_2 *capture capacity of amine-functionalized MOF-177 metal organic framework.* 2021. **9**(4): p. 105523.

[60]. Prakash, M., N. Sakhavand, and R.J.T.J.o.P.C.C. Shahsavari, H_2, N_2, *and* CH_4 *gas adsorption in zeolitic imidazolate framework-95 and-100: Ab initio based grand canonical Monte Carlo simulations.* 2013. **117**(46): p. 24407-24416.

[61]. Andas, J., M. Rahman, and M. Yahya. *Preparation and characterization of activated carbon from palm kernel shell*. in *IOP Conference Series: Materials Science and Engineering*. 2017. IOP Publishing.

[62]. Zhang, Z., et al., *Enhancement of* CO_2 *adsorption and* CO_2/N_2 *selectivity on ZIF-8 via postsynthetic modification.* 2013. **59**(6): p. 2195-2206.

[63]. Kapantaidakis, G., et al., *Gas permeation through PSF-PI miscible blend membranes.* 1996. **110**(2): p. 239-247.

[64]. Cai, Y., et al., *Gas transport property of polyallylamine–poly (vinyl alcohol)/polysulfone composite membranes.* 2008. **310**(1-2): p. 184-196.

[65]. Wang, D., K. Li, and W.J.J.o.M.S. Teo, *Polyethersulfone hollow fiber gas separation membranes prepared from NMP/alcohol solvent systems.* 1996. **115**(1): p. 85-108.

[66]. Li, J., et al., *Effect of polyethyleneglycol (PEG) on gas permeabilities and permselectivities in its cellulose acetate (CA) blend membranes.* 1998. **138**(2): p. 143-152.

[67]. Roh, E., et al., CO_2/N_2 *and* O_2/N_2 *Separation Using Mixed-Matrix Membranes with MOF-74 Nanocrystals Synthesized Via Microwave Reactions.* 2021. **42**(3): p. 459-462.

[68]. Chauhan, A. and P.J.J.A.B.T. Chauhan, *Powder XRD technique and its applications in science and technology.* 2014. **5**(5): p. 1-5.

[69]. Takagi, H., et al., *XRD analysis of carbon stacking structure in coal during heat treatment.* 2004. **83**(17-18): p. 2427-2433.

[70]. Clausen, B.S.J.C.t., *Combined (Q) EXAFS/XRD: technique and applications.* 1998. **39**(4): p. 293-300.

[71]. Bhargava, R., S.-Q. Wang, and J.L. Koenig, *FTIR microspectroscopy of polymeric systems*, in *Liquid chromatography/FTIR microspectroscopy/microwave assisted synthesis*. 2003, Springer Berlin Heidelberg Berlin, Heidelberg. p. 137-191.

[72]. Gallignani, M., et al., *Transmission FTIR derivative spectroscopy for estimation of furosemide in raw material and tablet dosage form.* 2014. **4**(5): p. 376-383.

[73]. Zaefferer, S.J.C.R. and Technology, *A critical review of orientation microscopy in SEM and TEM.* 2011. **46**(6): p. 607-628.

[74]. Alberti, G. and G. Nuzzaci, *1.6. 5 SEM and TEM techniques*, in *World Crop Pests*. 1996, Elsevier. p. 399-410.

[75]. Ozdemir, Y., N. Hasirci, and K.J.J.o.M.S.M.i.M. Serbetci, *Oxygen plasma modification of polyurethane membranes.* 2002. **13**: p. 1147-1152.

[76]. Bicalho, A., et al., *Incremental filling technique and composite material—Part I: Cuspal deformation, bond strength, and physical properties.* 2014. **39**(2): p. e71-e82.

[77]. Bahman, A., E.J.I.j.o.S. Alialhosseini, and Technology, *Change in hardness, yield strength and UTS of welded joints produced in St37 grade steel.* 2010. **3**(12): p. 1162-1164.

[78]. Pinnau, I., et al., *Gas permeation through composite membranes.* 1988. **37**(1): p. 81-88.

[79]. Salama, R.S., et al., *Adsorption, equilibrium and kinetic studies on the removal of methyl orange dye from aqueous solution by using of copper metal organic framework (Cu-BDC).* 2018. **10**(2): p. 195-207.

[80]. Ibrahim, A., et al., *Palladium nanoparticles supported on hybrid MOF-PRGO for catalytic hydrodeoxygenation of vanillin as a model for biofuel upgrade reactions.* 2016. **9**: p. 469-480.

[81]. Homayoonnia, S., S.J.S. Zeinali, and A.B. Chemical, *Design and fabrication of capacitive nanosensor based on MOF nanoparticles as sensing layer for VOCs detection.* 2016. **237**: p. 776-786.

[82]. Johnson, L.M., et al., *Elastomeric microparticles for acoustic mediated bioseparations.* 2013. **11**: p. 1-8.

[83]. Yang, J., et al., *Controlling nanodomain morphology of epoxy thermosets templated by poly (caprolactone)-block-poly (dimethylsiloxane)-block-poly (caprolactone) ABA triblock copolymer.* 2018. **8**(7): p. 3705-3715.

[84]. Hamouni, S., et al. *Alcohol and alkane organic extraction using pervaporation process*. in *Macromolecular Symposia*. 2019. Wiley Online Library.

[85]. Wang, Y., et al., *Electrochemical determination of 2, 4, 6-trinitrophenol using a hybrid film composed of a copper-based metal organic framework and electroreduced graphene oxide.* 2018. **185**: p. 1-9.

[86]. Cheng, J., et al., *Preparation of a Cu (BTC)-rGO catalyst loaded on a Pt deposited Cu foam cathode to reduce CO 2 in a photoelectrochemical cell.* 2018. **8**(56): p. 32296-32303.

[87]. Lin, G., et al., *Improved hydrophilicity from poly (ethylene glycol) in amphiphilic conetworks with poly (dimethylsiloxane).* 2009. **1**: p. 173-181.

[88]. Ansari-Asl, Z., et al., *Cu (II) metal-organic framework@ Polydimethylsiloxane nanocomposite sponges coated by chitosan for antibacterial and tissue engineering applications.* 2022. **336**: p. 111866.

[89]. Gong, X., et al., *ZIF-8-based membranes for carbon dioxide capture and separation.* 2017. **5**(12): p. 11204-11214.

[90]. Wang, H., et al., *A mechanically enhanced metal-organic framework/PDMS membrane for* CO_2/N_2 *separation.* 2021. **160**: p. 104825.

[91]. Li, H., et al., *Simultaneous enhancement of mechanical properties and* CO_2 *selectivity of ZIF-8 mixed matrix membranes: Interfacial toughening effect of ionic liquid.* 2016. **511**: p. 130-142.